UNCLASSIFIED
SECURITY CLASSIFICATION OF THIS PAGE

AD-A204 162

REPORT DOCUMENTATION PAGE

1a REPORT SECURITY CLASSIFICATION: UNCLASSIFIED	1b RESTRICTIVE MARKINGS
2a SECURITY CLASSIFICATION AUTHORITY	3 DISTRIBUTION/AVAILABILITY OF REPORT: Approved for public release, distribution unlimited
2b DECLASSIFICATION/DOWNGRADING SCHEDULE	
4 PERFORMING ORGANIZATION REPORT NUMBER(S)	5 MONITORING ORGANIZATION REPORT NUMBER(S): AFOSR-TR- 89-0081
6a NAME OF PERFORMING ORGANIZATION: Northwestern University	6b OFFICE SYMBOL (If applicable):
6c ADDRESS (City, State, and ZIP Code): Dept. of Materials Science & Engineering, Evanston, IL 60208	7a NAME OF MONITORING ORGANIZATION: Air Force Office of Scientific Research
	7b ADDRESS (City, State, and ZIP Code): Bolling AFB, Building 410, Washington, DC 20332-6448
8a NAME OF FUNDING/SPONSORING ORGANIZATION: AFOSR	8b OFFICE SYMBOL (If applicable): NE
8c ADDRESS (City, State, and ZIP Code): Bolling AFB, Building 410, Washington, DC 20332-6448	9 PROCUREMENT INSTRUMENT IDENTIFICATION NUMBER: AFOSR-85-0337 A & B
	10 SOURCE OF FUNDING NUMBERS: PROGRAM ELEMENT NO. 61102F; PROJECT NO. 2306; TASK NO A1; WORK UNIT ACCESSION NO. -

11 TITLE (Include Security Classification)

Investigation and Synthesis of High Temperature and Increased Stiffness RSP Aluminum Alloys

12 PERSONAL AUTHOR(S): Morris E. Fine and Julia R. Weertman

13a TYPE OF REPORT	13b TIME COVERED	14 DATE OF REPORT (Year, Month, Day)	15 PAGE COUNT
Final Technical	FROM 10/1/85 TO 9/30/88	November 15 1988	

16 SUPPLEMENTARY NOTATION

17 COSATI CODES			18 SUBJECT TERMS (Continue on reverse if necessary and identify by block number)
FIELD	GROUP	SUB-GROUP	Aluminum, high temperature alloys, aluminum-zirconium-vanadium, aluminum spinel

19 ABSTRACT (Continue on reverse if necessary and identify by block number)

The objective of this research was to investigate two promising systems as the basis for high temperature aluminum alloys useful to 425 C (800 F). The first is a metal matrix composite consisting of an aluminum-magnesium alloy matrix reinforced by spinel (magnesium aluminate) particulate. The second system is cubic tri-aluminum (zirconium, vanadium or titanium) dispersed in aluminum matrix. A mechanical alloying-liquid metal infiltration procedure for preparing specimens of the aluminum alloy matrix-spinel composite has been worked out and specimens with 4 vol.% spinel have been prepared. Also, 4 vol.% alumina composite samples were prepared for comparison. Spinel particles were within the aluminum alloy grains in contrast to the alumina which was at grain boundaries. The spinel composite had much better creep resistance at 410 C. Extrusions containing 5 vol.% tri-aluminum (0.75 vanadium, 0.25 zirconium) were prepared for this research by Lockheed-Palo Alto from rapidly solidified foil. The coarsening rate of the dispersed phase at 425 C was very low in keeping with the coherent interface and the measured creep rate at 425 C is much lower than in the current

20 DISTRIBUTION/AVAILABILITY OF ABSTRACT	21 ABSTRACT SECURITY CLASSIFICATION
☒ UNCLASSIFIED/UNLIMITED ☐ SAME AS RPT ☐ DTIC USERS	UNCLASSIFIED
22a NAME OF RESPONSIBLE INDIVIDUAL: Dr. Alan H. Rosenstein	22b TELEPHONE (Include Area Code): (202) 767-4933 / 22c OFFICE SYMBOL: NE

DD FORM 1473, 84 MAR — 83 APR edition may be used until exhausted. All other editions are obsolete.

SECURITY CLASSIFICATION OF THIS PAGE
UNCLASSIFIED

19. (Continued)

aluminum-iron-cerium alloy. An aluminum-vanadium intermetallic compound, however, forms at grain boundaries leading to a precipitate free zone which grows slowly at 425 C. Attempts to prepare samples with higher volume fractions of cubic $Al_3(Zr_{.25}V_{.75})$ dispersoids were unsuccessful due to the formation of the brittle $Al_{10}V$ intermetallic phase. Preliminary research was done on Al-Zr-Ti alloys. Cubic $Al_3(Zr_{.75}Ti_{.25})$precipitates were formed in a dilute alloy and these showed very high resistance to coarsening at 425 C. Further,alloys with 35 vol.% of tetragonal $Al_3(Zr_{.75}Ti_{.25})$ were remarkably ductile and could be cold rolled giving the possibility of developing a useful alloy by conventional ingot metallurgy.

FINAL REPORT

on

INVESTIGATION AND SYNTHESIS OF HIGH TEMPERATURE AND INCREASED STIFFNESS RSP ALUMINUM ALLOYS

covering period

1 October 1985 to 30 September 1988

by

Morris E. Fine and Julia R. Weertman

30 November 1988

This research was supported by the Department of the Air Force,
Air Force Office of Scientific Research under Grant No. AFOSR-85-0337
Electronic and Solid State Sciences Division
Bolling Air Force Base
Washington, DC 20332
Dr. Alan H. Rosenstein, Program Director

DEPARTMENT OF MATERIALS SCIENCE AND ENGINEERING
THE TECHNOLOGICAL INSTITUTE
NORTHWESTERN UNIVERSITY
EVANSTON, ILLINOIS 60208

PROFESSIONAL PERSONNEL

Professor Morris E. Fine, Principal Investigator

Professor Julia R. Weertman, Principal Investigator

Dr. Mahidhara K. Rao, Postdoctoral Research Associate, 2/1/86 - 6/15/87

Dr. V. R. Parameswaran, Research Fellow, 10/5/87 - 9/20/88

Dr. Yen-Cheng (Dan) Chen, Ph.D. student, Graduate Research Assistant, 10/1/85 - 4/15/88

Mr. Terry S. Creasy, M.S. student, 10/1/85 - 7/31/87

Mr. John J. Blum, Ph.D. student, Graduate Research Assistant, 9/16/87 - 9/30/88

Mr. Philip A. Earvolino, Ph.D. student, Graduate Research Assistant, 6/8/88 - 8/18/88

SUMMARY

The objective of this research was to investigate two promising systems as the basis for high temperature aluminum alloys useful to 425°C (800°F). The first is a metal matrix composite consisting of an aluminum-magnesium alloy matrix reinforced by spinel (magnesium aluminate) particulate. The second system is $Al_3(ZrX)$, where X is V or Ti dispersed in aluminum matrix. Here the lattice parameter of the $Al_3(ZrX)$ intermetallic particles nearly matches that of the matrix. Research on dilute alloys has shown a low coarsening rate for these intermetallics at 425°C. A study of aluminum alloys with a higher concentration of zirconium and vanadium was completed.

A mechanical alloying-liquid metal infiltration procedure for preparing specimens of the aluminum alloy matrix-spinel composite has been worked out and specimens with 4 vol.% spinel have been prepared. Also, 4 vol.% alumina composite samples were prepared for comparison. Spinel particles are located inside the aluminum alloy grains, whereas the alumina particles are primarily situated at grain boundaries. The creep resistance at 410°C of the spinel composite is much better than that of the alumina composite.

Extrusions containing 5 vol.% $Al_3(V_{.75}Zr_{.25})$ were prepared for this research by Lockheed-Palo Alto from rapidly solidified foil. The measured creep rate at 425°C is much lower than that of the current aluminum-iron-cerium alloys. An aluminum-vanadium intermetallic compound, however, forms at grain boundaries leading to a precipitate free zone which grows slowly at 425°C. Dilute alloys containing 1 vol.% $Al_3(ZrTi)$ were then prepared and these show more promise than the aluminum-zirconium-vanadium alloys.

INTRODUCTION

By analogy with Ni-base superalloys, which are useful to 0.75 T_m (T_m is the absolute melting temperature of Ni), one may anticipate development of an Al base alloy useful to approximately 425°C or 800°F. In order to develop a successful Al alloy for use at such a temperature, many basic principles must be considered. Such an alloy may owe its strength at high as well as room temperature to a uniform dispersion of second phase particles which are coherent or semi-coherent with the matrix. To test this theory, two systems were studied:

1. A composite of Al-Mg alloy matrix and $MgAl_2O_4$ dispersoid
2. A dispersion of $Al_3(Zr,X)$ in Al

Both of these systems were selected on the basis of lattice matching between an Al alloy matrix and the dispersed phase. Preliminary work was done on Al-Al_3Zr and Al-$Al_3(Zr,V)$ under AFOSR Grant No. 82-0005 and the results on dilute alloys were very promising. The present research on Al-5 vol.% ($Zr_{.25}V_{.75}$) shows great promise; however, incoherent $Al_{10}V$ was found to form on grain boundaries in the more concentrated alloys which leads to adjacent precipitate free zones which increase in width on aging. Therefore research was begun on Al-Zr-Ti alloys, which won't have this problem. Results on a dilute Al-$Al_3(Zr,Ti)$ alloy showed an even lower particle coarsening rate for the metastable cubic phase than a comparable Al-$Al_3(Zr,V)$ alloy. Further, an alloy with approximately 30 vol.% of the stable tetragonal phase was sufficiently ductile that it could be cold rolled, a very interesting finding.

PROGRESS AND RESULTS

1. Al-Mg Alloy matrix-$MgAl_2O_4$ spinel composite

The cubic spinel, nominal composition $MgAl_2O_4$, appears to be a better candidate oxide for the dispersion strengthening of Al than the hexagonal oxide α-Al_2O_3. The lattice parameter of stoichiometric $MgAl_2O_4$ is 8.083Å, which is almost twice that of Al, 4.0496Å. Thus a semicoherent interface may be anticipated. Furthermore, at least one spinel-structured oxide exhibits some ductility at room temperature. If the dispersed spinel particles in the Al alloy matrix have even very limited ductility, the composite should have a much better fracture toughness than one with particles like α-Al_2O_3 or SiC, which behave in a very brittle fashion. Also, spinel has a better developed cleavage habit than α-alumina and thus a more uniform mixture by mechanical alloying is expected. Since the elastic constants of spinel are considerably larger than those of Al, improved stiffness as well as improved high temperature strength are expected from dispersing spinel in an Al alloy matrix.

A procedure for preparing creep and elevated temperature fatigue specimens of Al-Mg alloy matrix-spinel ($MgAl_2O_4$) or corundum (α-Al_2O_3) dispersions has been developed. Al-3% Mg rapidly solidified powder for the matrix was kindly provided for this research by the Alcoa Technical Center. Commercially available spinel and α-Al_2O_3 powders were provided by Baikowski. Composites containing 4 vol.% of either oxide were prepared by mechanical alloying with 1 wt.% oleic acid as a "grinding" aid using alumina pellets as the "grinding" medium. The mechanically alloyed powders were cold pressed to 0.75 in diameter discs with a dual action die at 350 MPa pressure. The cold pressed pellets and dies were heated to 710°C for 5 minutes for liquid metal infiltration and then pressure forged in a platen press heated to 140°C to form discs 20 mm diameter and

2 mm thick. The pressure forged discs were then cold rolled to 0.8 mm thickness with intermediate anneals at 600°C. The final densities were in the range 99 to 100% of the theoretical. The specimens were cut using electro-discharge machining.

Transmission electron microscopy showed that the dispersion of the spinel particles in the Al-3% Mg matrix was much better than that of the α-alumina particles. The former were dispersed within grains while the latter were at grain boundaries, having pinned them during recrystallization. This difference in the siting of the particles in itself may be an indication that the matrix/spinel interface has lower energy than the matrix/α-alumina interface. The alumina particles (150-300 μm diameter) were much larger than the spinel particles (30-150 μm). The former were not reduced in size by the mechanical alloying. However, in both cases the distribution of particles was uneven. This resulted in uneven grain size.

Tensile tests were conducted at room temperature and creep tests at 410°C. The ultimate tensile stress of the Al-3% Mg-4 vol.% spinel was 235 MPa while the elongation to fracture was 15%. For Al-3% Mg-4 vol.% α-alumina, the UTS was 210 MPa with 9% elongation to fracture. Better properties can no doubt be achieved with more uniform particle dispersions and smaller particle size.

The creep results at 410°C are summarized in Table 1.

TABLE 1.

Steady state creep data for Al-3% Mg-4 vol.% spinel and Al-3% Mg-4 vol.% α-alumina metal matrix composites

Stress MPa	Strain Rate (sec^{-1}) Al-spinel	Al-alumina
17	-	1.3×10^{-6}
22	2×10^{-6}	26×10^{-6}
30	105×10^{-6}	990×10^{-6}
35	624×10^{-6}	-

The creep resistance of the Al-spinel metal matrix composite (MMC) at 410°C is clearly better than that of the Al-alumina MMC. This is at least in part due to the more uniform particle dispersion achieved in the former composite.

The research results with the 4 vol.% oxide metal matrix composites are reported in the M.S. thesis of Terry Creasy and a paper, "Al Alloy with Spinel for Oxide Dispersion Strengthening". The latter is Appendix A to this report.

Achievement of the desired high strengths and creep resistance will require a higher volume fraction of particles. Efforts were made to prepare Al-3% Mg metal matrix composites with 10 vol.% spinel and 10 vol.% α-Al_2O_3 using the same procedure as with 4 vol.% of each. Limited success was achieved. Better equipment is needed than was available at Northwestern. The results, however, justify additional research on the Al-spinel MMC system.

2. Al-Al_3(V,Zr) dispersions

A remarkably slow volumetric coarsening rate of 1.0×10^{-28} m^3/h at 425°C was found for the metastable cubic Ll_2 structured $Al_3(Zr_{.25}V_{.75})$ in 5 vol.% precipitate melt spun ribbons prepared for this research by Lockheed. However a region depleted of Ll_2 precipitates, i.e., a precipitate free zone (PFZ), forms along the grain boundaries during aging due to formation at the grain boundaries of the stable phases, mainly $Al_{10}V$. It was also found that the PFZ width increases with aging time. In order to understand the growth mechanism for the Ll_2 phase as well as that for the PFZ, detailed studies were undertaken of the same ribbons, i.e., Al-5 vol.% $Al_3(Zr_{.25}V_{.75})$ alloy, aged at different temperatures.

Figure 1 shows the coarsening results of the Ll_2 precipitates at 425, 450 and 500°C, where the cube of the average particle radius, r_t,

is plotted against aging time, t. The linear correlation coefficient, R, and the slope for each best fitting line are given in Table 2. A linear

TABLE 2.

Measured coarsening rate constant, K, and coefficient of linearity, R, for Ll_2 $Al_3(Zr_{.25}V_{.75})$ precipitates at 425, 450 and 500°C.

Temperature (°C)	K (m^3/hr)	R
425*	1.03×10^{-28}	0.997
450*	6.13×10^{-28}	0.997
500	1.28×10^{-26}	0.996

* Specimens were preaged at 500°C for 2.5 hrs. to prevent cellular precipitation.

relationship between the cube of $\bar{r}_t$ and t seems well satisfied. An LSW volume diffusion controlled process described by Eq.(1) seems to be the growth mechanism for the Ll_2 structured $Al_3(Zr_{.25}V_{.75})$ precipitates.

$$\bar{r}_t^3 - \bar{r}_o^3 = \frac{12.8\sigma D V_m^2 C_\infty}{9RT} t = Kt \ . \qquad (1)$$

Here $\bar{r}_o$ is a constant, σ is the interfacial energy, V_m is molar volume, D is bulk diffusion coefficient of the rate controlling solute and C_∞ is its concentration in the matrix far from the interface. The activation energy for the particle coarsening, Q_c', can be calculated from Eq.(1) from the plot of $\ln(KT/V_m^2 C_\infty \sigma)$ vs the reciprocal of RT. To a first order approximation, the factors C_∞, V_m and σ are assumed to be constant in the temperature range from 425°C to 500°C. This is a good assumption for the last two terms. Q_c is calculated to be 294 KJ/mole. This value is closer to the activation energy for diffusion of Zr in Al than that of V in Al, 242 and 82 KJ/mole, respectively. Consequently, the volume diffusion of

Zr is thought to be the rate controlling process for the Ostwald ripening of the $L1_2$ phase. Furthermore, Q_c is corrected to 230 KJ/mole after considering the temperature dependence of C_∞. This value is even closer to the activation energy for Zr diffusion in Al. The above results are self-consistent suggesting that the coarsening kinetics of the $L1_2$ phase is an LSW volume diffusion controlled process.

The growth kinetics of the PFZ at 425, 450 and 500°C were investigated and the results are summarized in Fig. 2, where the PFZ half-width, $W_{PFZ}/2$, is plotted vs square root of the annealing time as done by Jensrud and Ryum for Al-Li alloys. According to these authors, the growth behavior of the PFZ in an Al-Li alloy which has a similar microstructure to the present Al-Zr-V alloy can be described by the following equation,

$$W_{PFZ}/2 = b(Dt)^{\frac{1}{2}} , \qquad (2)$$

where D is the diffusivity of solute in Al and b is a complicated function of the alloy composition and the solute contents in the Al matrix adjacent to the both sides of the PFZ. Using the same procedure as done previously for coarsening of the $L1_2$ phase, the activation energy for the PFZ growth is calculated to be 285 KJ/mole by taking b as a constant since it is only a slowly varying function of the solute concentration in the Al matrix in the temperature range concerned here. The calculated activation energy indicates that PFZ growth in the present alloy is also controlled by the volume diffusion of Zr, not V, in the Al matrix. The grain boundary precipitates are, however, mainly $Al_{10}V$. A possible explanation is given as follows. Since V diffuses faster than Zr in Al at the aging temperature, as soon as $L1_2$ particles dissolve, vanadium diffuses toward the grain boundaries and it leaves a local matrix with a high Zr content

behind. The further dissolution of other Ll_2 particles will be retarded until this excess of Zr diffuses to the grain boundaries to form Al_3Zr or to partition into the $Al_{10}V$ as a solute. As a result, the final growth rate of PFZ is determined by the volume diffusion of Zr in Al. This leads to the promising result that the PFZ will grow only slowly at the application temperature of interest for this alloy.

In the present alloy, most of grain boundary precipitates are $Al_{10}V$. High resolution transmission electron microscopy (HRTEM), as shown in Fig. 3, disclosed that micro-twins and stacking faults are frequently observed in this phase. The average intercept length, $\bar{L}$, the volume fraction, $\emptyset$, of the grain boundary precipitates and grain size D after various aging times were measured by quantitative metallography. The results are listed in Table 3. Basically, the volume fraction $\emptyset$ increases

TABLE 3.

Changes of average intercept length, $\bar{L}$, volume fraction, $\emptyset$, of grain boundary precipitates, and grain size, D, in alloy ribbon with aging time at 425°C.

Aging Time (hours)	$\bar{L}$ (μm)	$\emptyset$	D (μm)
0	0.18	0.023	3.4
200	0.25	0.031	3.53
400	0.32	0.034	3.7
800	0.34	0.039	3.8
1200	0.35	0.041	4.0

linearly with square root of aging time. However, since grain size does not increase much (less than a 10% increase after 1200 hours of exposure at 425°C following a preaging at 500°C for 2.5 hours), the $Al_{10}V$ particles forming along the grain boundaries have the positive effect of preventing

grain growth.

Figure 4 is an HRTEM image of an Ll_2 particle aged at 600°C for 1.5 hours. The atomic image of the Ll_2 phase is clearly distinguishable from the matrix. The ordered structure of the Ll_2 phase still remains after exposure at this high temperature. It is also shown that the interface between the Ll_2 particle and Al matrix is fully coherent. However, a fault structure proven to be an anti-phase domain boundary is formed inside the Ll_2 particles, as shown in Fig. 5. This anti-phase boundary can be caused by coalescence of two out-of-phase Ll_2 particles or by the shear produced by a dislocation on {100} planes.

The growth kinetics at 425°C of the Ll_2 particles in extruded bars, also prepared by Lockheed, are similar to the growth kinetics in the melt spun ribbons. The results are shown in Fig. 6, from which a volumetric growth rate of 1.1 X 10^{-28} m^3/h is calculated. It was also found that creep at 425°C increases the growth rate of the Ll_2 particles by around 50%. Figure 7 presents the creep results. The worst test result (i.e., fastest creep rate) for each alloy is given. High temperature tensile tests carried out at 425°C reveal that the yield strengths of alloys 2 (Al-$Al_3(V_{.25}Zr_{.75})$) and 4 (Al-$Al_3(V_{.75}Zr_{.25})$) are 14 and 40 MPa respectively. Apparently, the poor creep properties observed in alloy 2 are due to its weak strength at 425°C. Detailed microstructural studies found that more coarse equilibrium phase particles, around 1-5 μm in size, are present in alloy 2 than are present in alloys 3 (Al-$Al_3(V_{.50}Zr_{.50})$) and 4. This is suggested to be one of the reasons why alloy 2 is so weak. Alloy 2, with its high Zr content, has a higher melting temperature, which makes it more difficult to process by rapid solidification.

It should be pointed out that Al-Mg with 4 vol.% spinel has better

creep resistance than the Al-4 vol.% $Al_3(Zr_{.25}V_{.75})$ extruded bar (alloy 4). These results are more fully presented in the Ph.D. thesis of Yen-Cheng Chen and in the paper, "Microstructural Evolution and Mechanical Properties of Rapidly Solidified Al-Zr-V Alloys at High Temperatures", which has been submitted to Acta Metallurgica for publication. The latter is Appendix B to this report.

More concentrated Al-Zr-V alloys designed to contain 15 and 25 vol.% Ll_2 phase were made by Lockheed by melt spinning. TEM observations disclosed that a large amount of coarse $Al_{10}V$ particles, around 1 μm in size, exist in the as-quenched 25 vol.% alloy. Their presence causes these ribbons to be brittle. The 15 vol.% ribbons are ductile even though many $Al_{10}V$ phase particles were observed after quenching, but their sizes are generally smaller, around 0.1 μm. The spherical Ll_2 phase precipitates out in the 15 vol.% alloy after aging at 500°C. However the amount of Ll_2 phase is less than in the previous 5 vol.% ribbons. This is because less solutes remained dissolved in the matrix after quenching due to $Al_{10}V$ formation in the ribbons. Apparently, a rapid solidification process having a higher quenching rate than the process used at Lockheed in the present study is required to produce a more concentrated and useful alloy.

3. Al-Al_3(Zr,Ti) dispersions

Because of the problem of $Al_{10}V$ precipitates at grain boundaries and the attendant Ll_2 precipitate free zone, it was decided to investigate Al-Zr-Ti alloys. From this point of view Al-Zr-Ti alloys are more promising since the stable tetragonal phase in this system matches the aluminum lattice rather well and it is not expected to form at grain boundaries as readily as does $Al_{10}V$. Thus it is of interest to compare the rate of Ostwald ripening of Ll_2-structured Al_3(Zr,Ti) with that of Al_3(Zr,V).

Alloys containing 1 vol.% of $Al_3(Zr_{.75}Ti_{.25})$ were prepared, and the growth of the Ll_2-structured precipitates during high temperature aging was studied.

Small quantities (about 4 g) of alloys formulated to contain 1 vol.% of $Al_3(Zr_{.75}Ti_{.25})$ were arc melted under argon atmosphere using a water cooled copper crucible and a non-consumable tungsten electrode. This procedure was followed in previous studies of Al-Zr-V alloys. The microstructure of the as-cast alloy did not show any precipitates on the chilled side of the cast buttons, indicating that the solutes were in metastable solid solution in the aluminum.

Thin slices (about 0.5 mm in thickness) were cut from the buttons using a diamond saw. These slices were given a pre-aging treatment at 500°C for one hour in order to prevent cellular precipitation during subsequent aging, as was done previously with the arc melted Al-Zr-V alloys containing 1 vol.% of Ll_2 precipitates. The pre-aged samples were held at 425°C for different times up to 600 hours. All aging was carried out under vacuum (better than 10^{-3} Pa); the temperature was maintained at 425 ± 1°C. After aging, foils were prepared and examined in an electron microscope.

Figure 8 shows the Ll_2 spherical precipitates after aging at 425°C for 200, 400, and 600 hours. Figure 9 compares the variation of particle radius as a function of aging time in the present alloy with that observed earlier in the Al-Zr-V alloy containing 1 vol.% $Al_3(Zr_{.125}V_{.875})$.

The precipitate sizes in the present Al-Zr-Ti alloy are much smaller than those observed in Al-Zr and Al-Zr-V alloys prepared under conditions thought to be identical. The scatter in the precipitate sizes increased with increasing aging times; however, even the largest particles in the Al-Zr-Ti alloy, after aging for 600 hours at 425°C, are smaller than the

average size in the Al-Zr-V alloy after 400 hours aging. Some particles grew faster than others. This is due in part to enhanced diffusion along dislocations. Particles near or attached to dislocations are larger. Also, an inhomogeneous distribution of solute plays a role. Many precipitates appear to be along bands, and the particle radii seem to be larger here than those not on bands.

Because the $L1_2$ particle sizes appear to be smaller in an Al-Zr-Ti alloy than in a similar Al-Zr-V alloy while the particle growth rates at 425°C are comparable, and because the harmful grain boundary particles such as $Al_{10}V$ are absent in the Al-Zr-Ti alloys, this latter seems to be the more promising system for high temperature applications. A paper describing these results has been accepted for publication by Scripta Metallurgica and is Appendix C of this report.

Alloys containing tetragonal DO_{23} $Al_3(Zr_{.75}Ti_{.25})$ or $Al_3(Zr_{.5}Ti_{.5})$ particles are remarkably ductile. Arc melted buttons containing up to 35 vol.% of the particles have been cold rolled with intermediate anneals. Plates 10 mm thick were cold rolled to 0.6 mm without cracking. In an alloy containing 15 vol.% $Al_3(Zr_{.75}Ti_{.25})$, the DO_{23} phase as cast was in the form of needles of 0.01 mm average diameter and 0.2 mm average length, but after the cold reduction the needles were on the average 0.005 mm in diameter and 0.04 mm long. Figures 10a and b compare the as cast and cold worked structures. Note the DO_{23} fibres in Fig. 10b are oriented in the rolling direction. The reduction in diameter of the fibres indicates they possess ductility. Their Knoop hardness is 700 kg/mm^2. This alloy system, therefore, shows promise of producing a useful metal matrix composite by conventional casting and thermechanical processing. One may envision the aluminum equivalent of piano wire, which is one of the strongest materials known to man.

LIST OF PUBLICATIONS -- AF SUPPORTED

1. L. Angers, Y. Chen, M. E. Fine, J. R. Weertman and M. S. Zedalis, "Rational Design of High Temperature Aluminum Alloys" in Conference Proceedings, Aluminum Alloys - Their Physical and Mechanical Properties, Vol. I, E. A. Starke, Jr. and T. H. Sanders, Jr. (eds.) Engineering Advisory Services Ltd.(Chameleon Press Ltd., London, U.K., 1986) pp. 321-337.

2. M. S. Zedalis and M. E. Fine, "Precipitation and Ostwald Ripening in Dilute Al Base-Zr-V Alloys", Metall. Trans. 17A (1986) 2187.

3. L. M. Angers, L. D. Marks and J. R. Weertman, "A Quasicrystalline Decagonal Phase in Al-Fe-Ce" in Mat. Res. Soc. Symposium Proceedings Vol. 62, Materials Research Society (1986) pp. 255-262.

4. M. E. Fine, Y. Chen, J. Conley and J. Caputi, "Interface Adsorption and Ostwald Ripening", Scripta Metall. 20 (1986) 743.

5. L. Angers, M. E. Fine and J. R. Weertman, "Effect of Plastic Deformation on the Coarsening of Dispersoids in a Rapidly Solidified Al-Fe-Ce Alloy", Metall. Trans. 18A (1987) 555.

6. R. E. Lewis, D. D. Crooks, Y. C. Chen, M. E. Fine and J. R. Weertman, "High Temperature Al-Zr-V Alloys Using Rapid Solidification Processing", Proceedings of 3rd Intl. Conf. on Creep and Fracture of Engineering Materials and Structure, B. Wilshire and R. W. Evans (eds.) The Institute of Metals, London (1987) pp. 331-346.

7. Y. C. Chen, M. E. Fine, J. R. Weertman and R. E. Lewis, "Coarsening Behavior of $L1_2$ Structured $Al_3(Zr_xV_{1-x})$ Precipitates in Rapidly Solidified Al-Zr-V Alloy", Scripta Metall. 21 (1987) 1003.

8. T. S. Creasy, "Oxide Dispersion-Strengthening of Al-3% Mg with Spinel and Alumina", M.S. Thesis, Northwestern University, Dept. of Materials Science & Engineering, Evanston, IL, 1987.

9. T. Creasy, J. R. Weertman and M. E. Fine, "Aluminum Alloy with Spinel for Oxide Dispersion Strengthening", to appear in TMS Symposium Volume, Dispersion Strengthened Aluminum Alloys (TMS Annual Meeting, Phoenix, AZ, 25-28 January 1988). In press.

10. M. E. Fine, "Stability and Coarsening of Dispersoids in Aluminum Alloys", to appear in TMS Symposium Volume, Dispersion Strengthened Aluminum Alloys (TMS Annual Meeting, Phoenix, AZ, 25-28 January 1988). In press.

11. Y. C. Chen, M. E. Fine and J. R. Weertman, "Microstructural Evolution and Mechanical Properties of Rapidly Solidified Al-Zr-V Alloys at High Temperatures". Submitted to Acta Metallurgica.

12. V. R. Parameswaran, J. R. Weertman and M. E. Fine, "Coarsening Behavior of $L1_2$ Phase in an Al-Zr-Ti Alloy". To appear in January 1989 issue of Scripta Metallurgica.

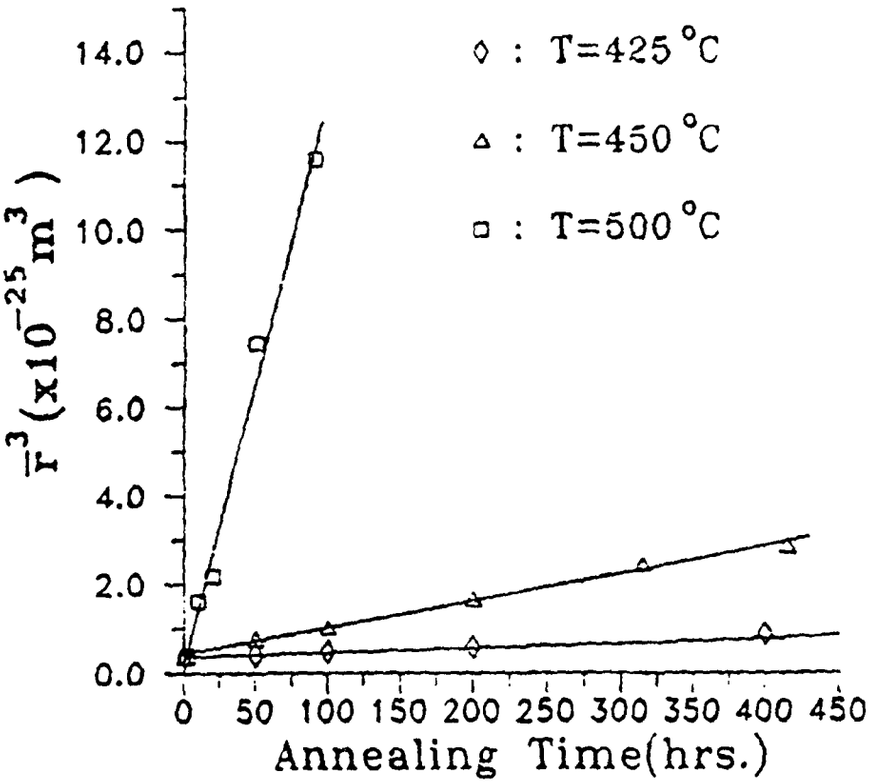

Figure 1. Coarsening kinetics of Ll_2 $Al_3(Zr_{.25}V_{.75})$ precipitates at 425, 450 and 500°C, after a pre-treatment of 2.5 hours at 500°C in 4 vol.% precipitate alloy (alloy No. 4).

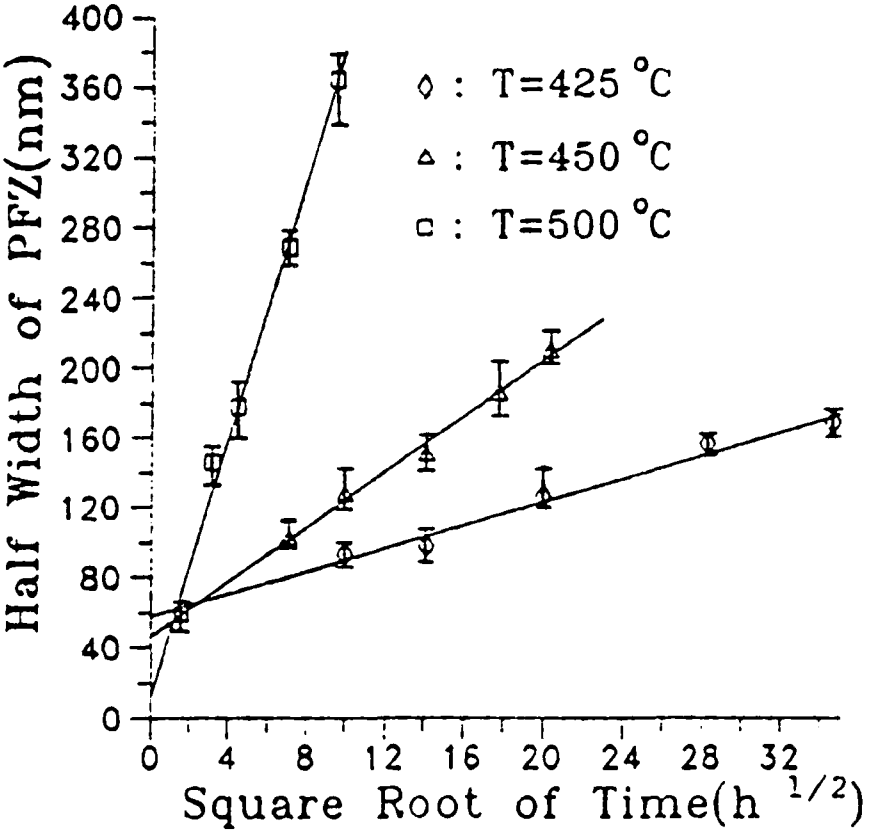

Figure 2. Growth kinetics of PFZ at 425, 450 and 500°C, after a pre-treatment of 2.5 hours at 500°C (alloy No. 4).

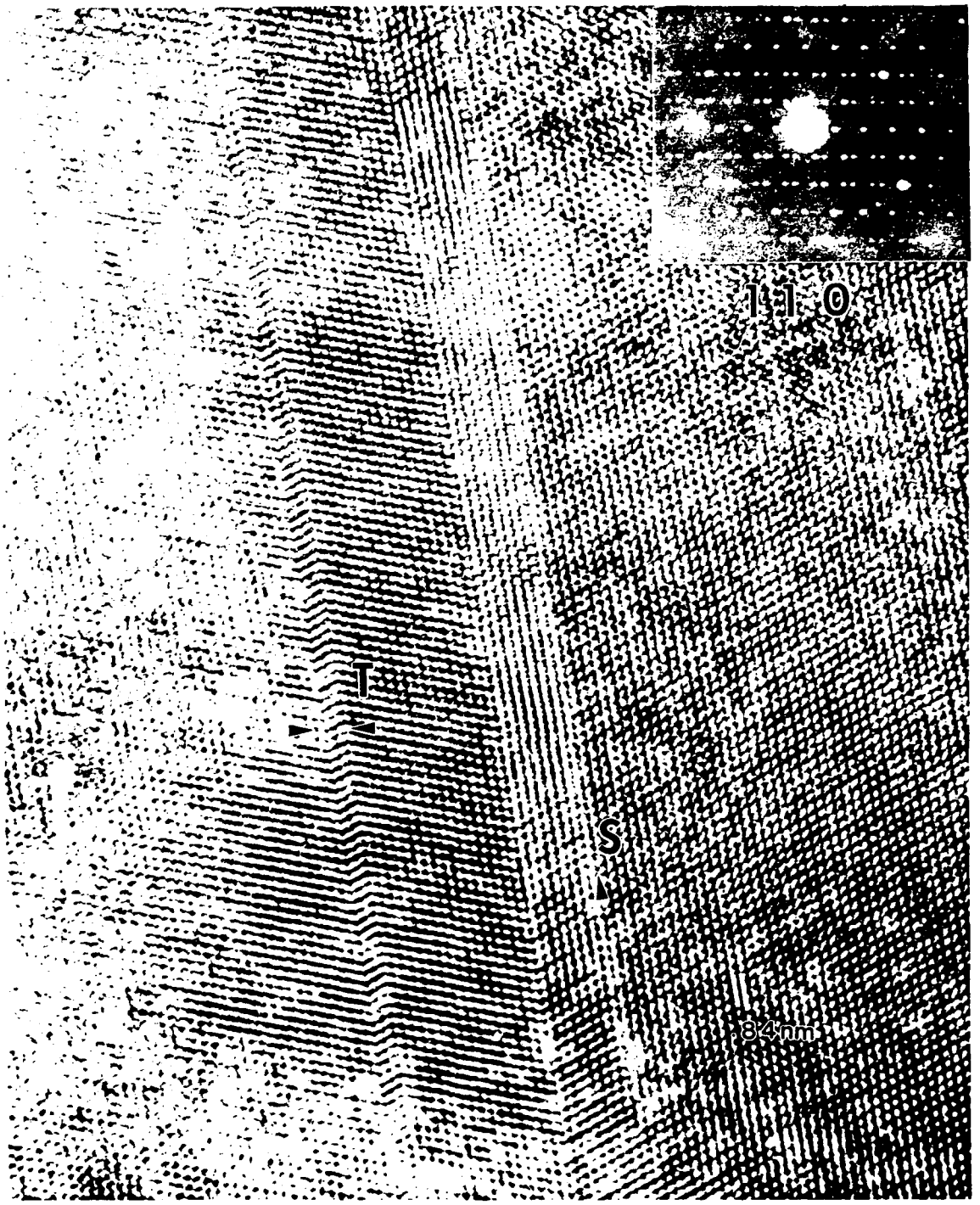

Figure 3. High resolution TEM image of grain boundary $Al_{10}V$ phase, where a macro-twin indicated by letter T and a stacking fault indicated by letter S are observed. It was taken close to (110) zone axis.

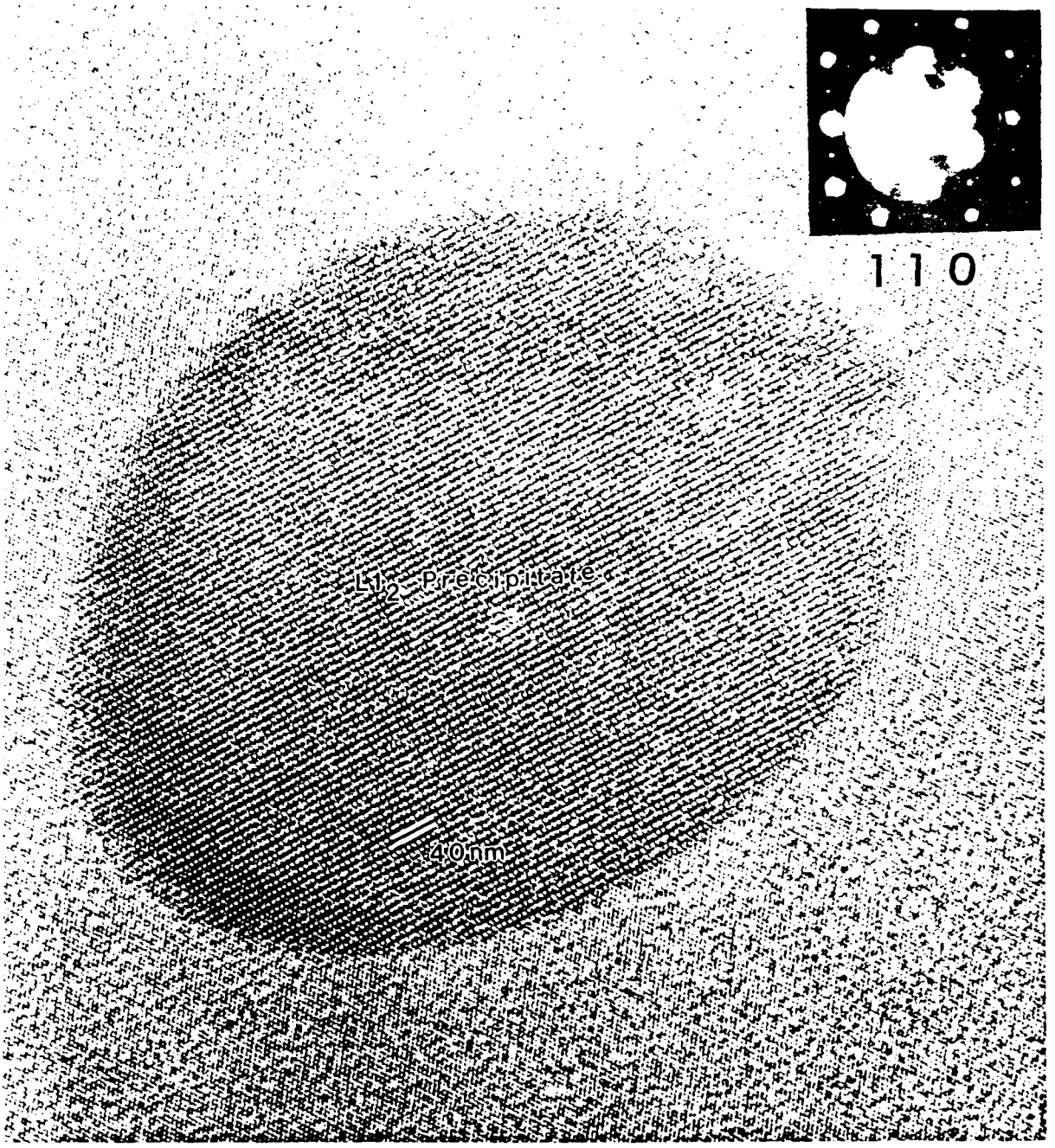

Figure 4. High resolution TEM image of $L1_2$ precipitate, which was taken close to (110) zone axis.

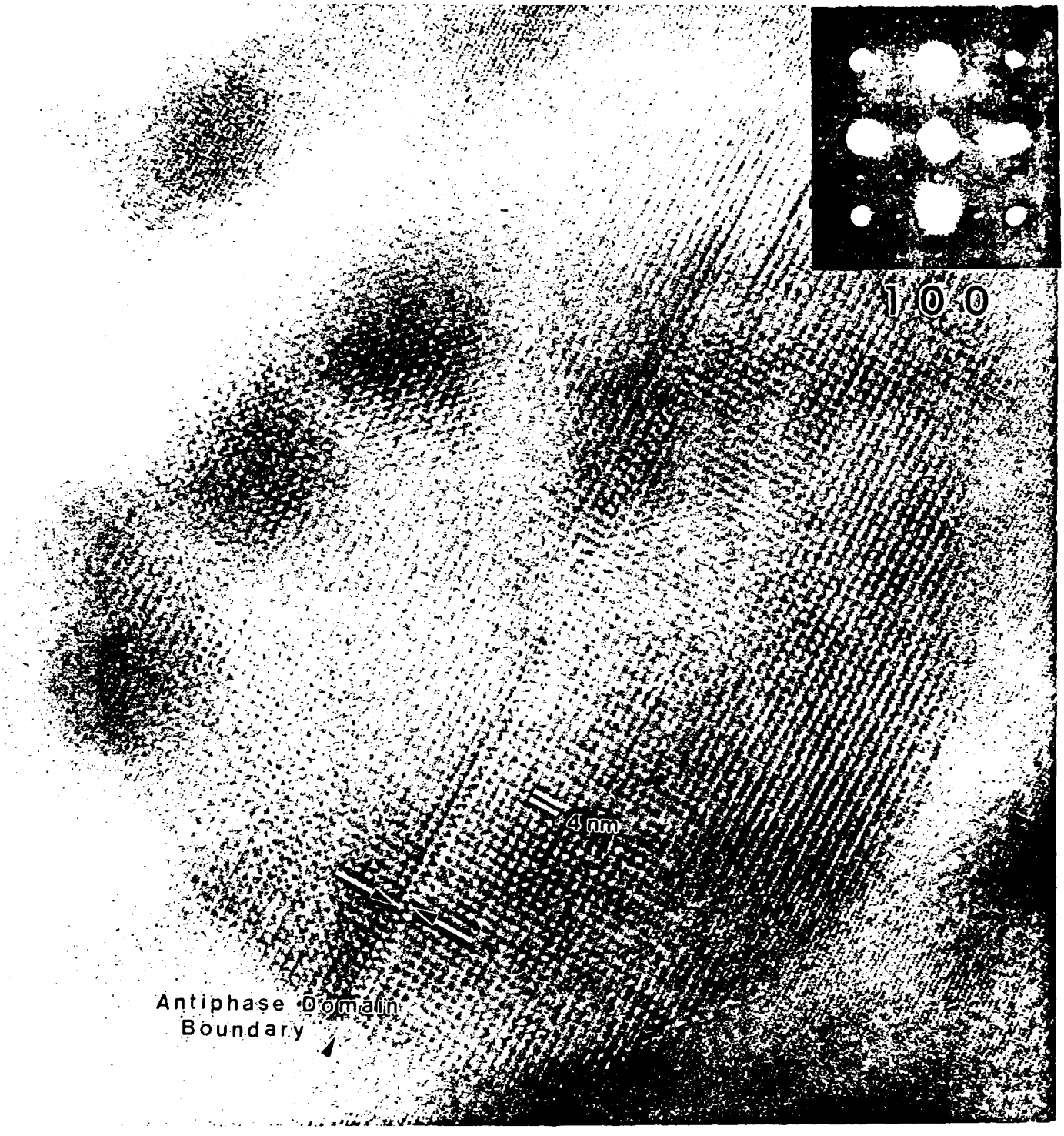

Figure 5. High resolution TEM image of $L1_2$ precipitate, within it an anti-phase domain boundary is present. It was taken close to (100) zone axis.

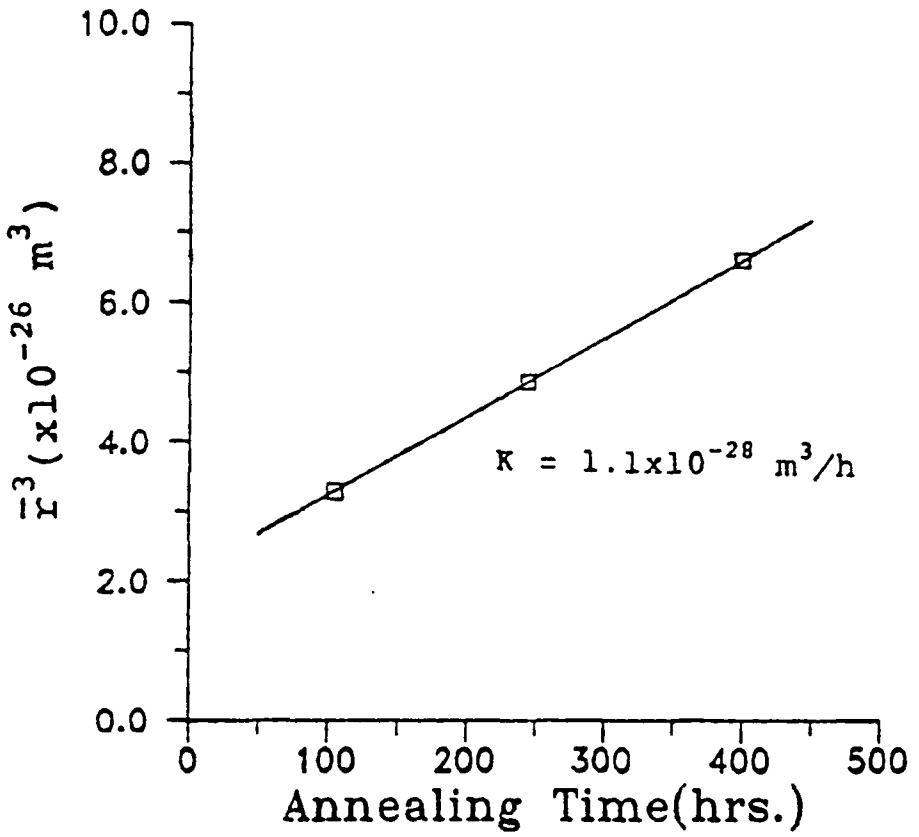

Figure 6. Growth kinetics of $L1_2$ phase at 425°C in extruded bar.

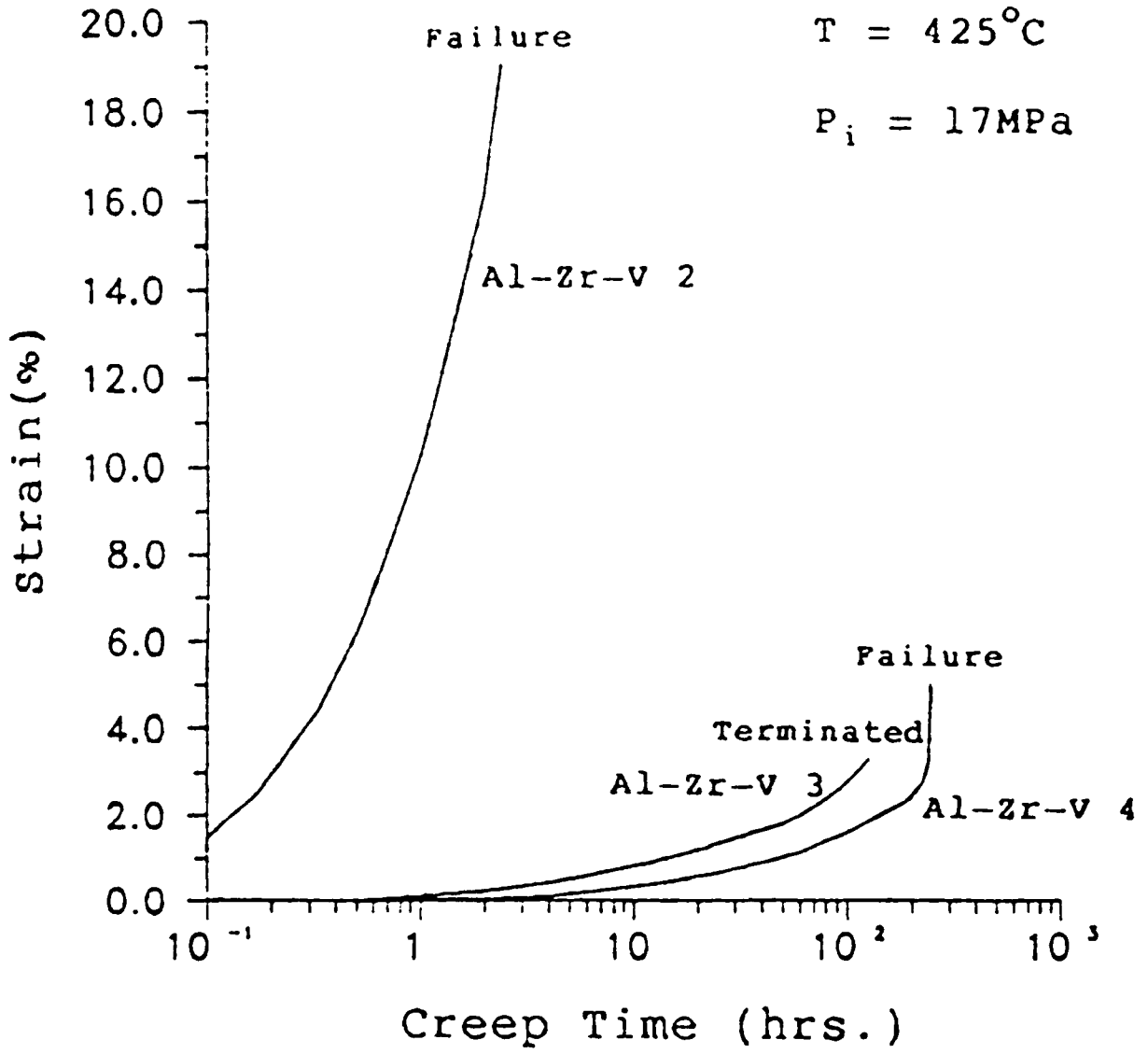

Figure 7. Creep results of Al-Zr-V alloys at 425°C.

Alloy 2: Al + 5 vol.% $Al_3(Zr_{.75}V_{.25})$

Alloy 3: Al + 5 vol.% $Al_3(Zr_{.50}V_{.50})$

Alloy 4: Al + 5 vol.% $Al_3(Zr_{.25}V_{.75})$

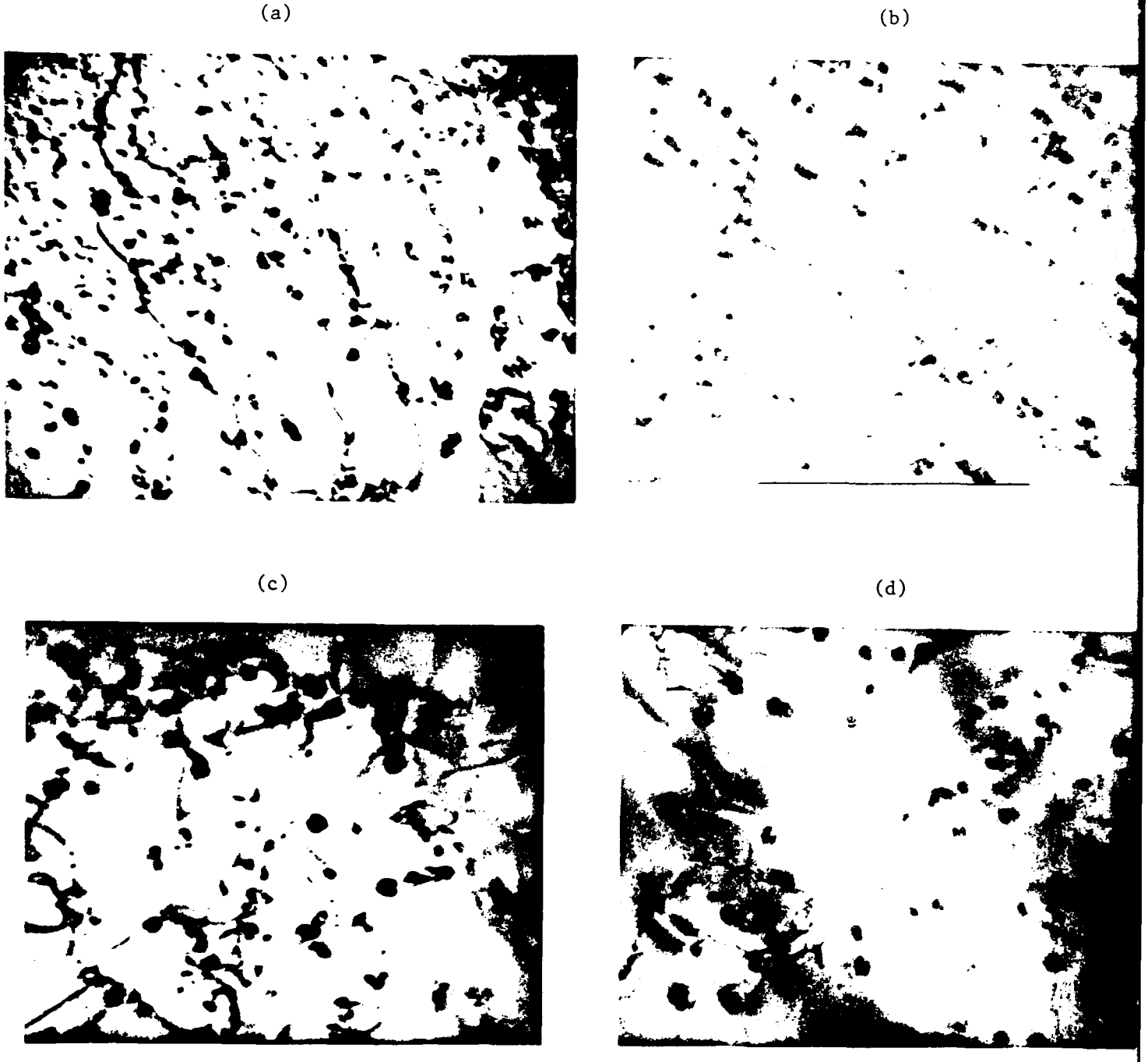

Figure 8. $L1_2$ precipitates in an Al-Zr-Ti alloy containing 1 vol.% $Al_3(Zr_{.75}Ti_{.25})$ after aging for various times. All samples were pre-aged at 500°C for one hour.

(a) 200 hours, (b) and (c) 400 hours, and (d) 600 hours

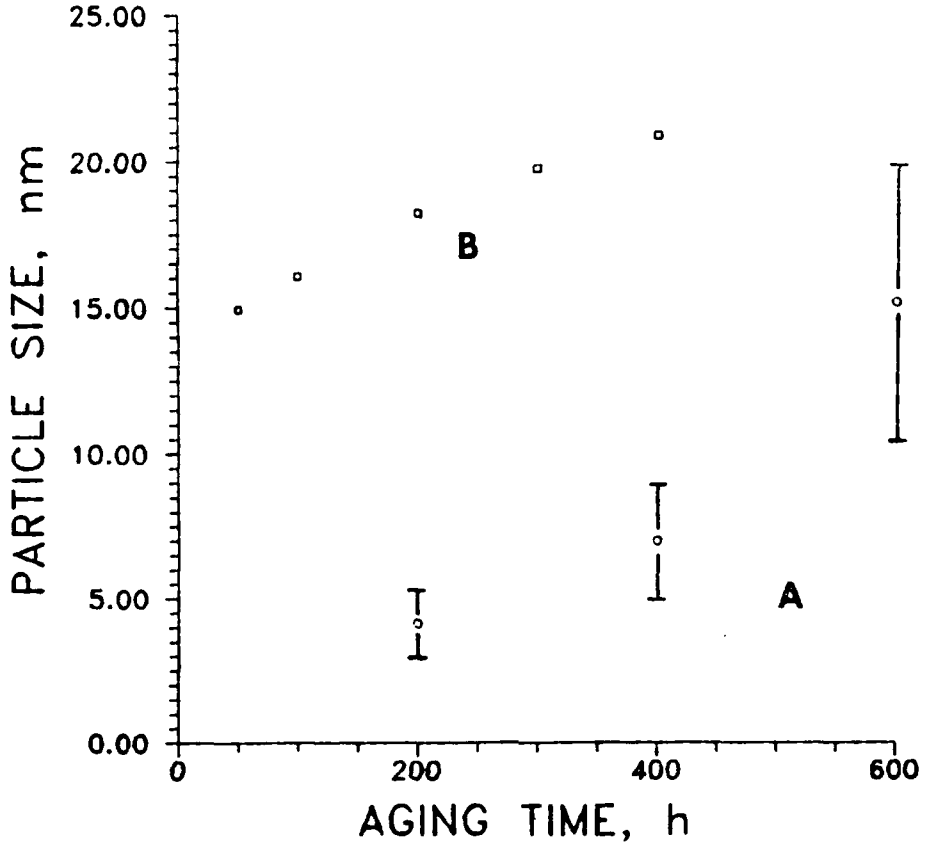

Figure 9. Variation of Ll_2 average particle radius, $\bar{r}$, with aging time at 425°C.

A: Present results in Al-1 vol.% $Al_3(Zr_{.75}Ti_{.25})$, arc melted.
B: Al-1 vol.% $Al_3(Zr_{.125}V_{.875})$, arc melted.

All samples were pre-aged at 500°C for one hour.

Figure 10(a). As cast microstructure of a Al-Zr-Ti alloy containing 15 vol.% $Al_3(Zr_{.75}Ti_{.25})$ dispersoid. (300X).

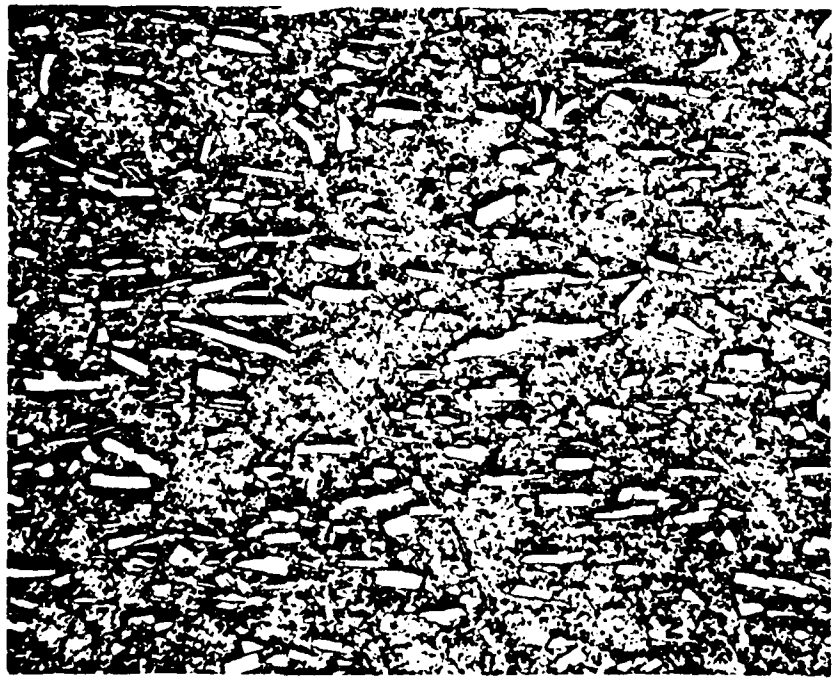

Figure 10(b). Rolled structure with the dispersoids aligned in the rolling direction. (240X).

APPENDIX A

To appear in TMS Symposium Volume, Aspects of Strengthened Aluminum Alloys (TMS Annual Meeting, Phoenix, AZ, 25-28 January 1988).

ALUMINUM ALLOY WITH SPINEL FOR OXIDE DISPERSION STRENGTHENING*

T. Creasy, J. R. Weertman and M. E. Fine

Department of Materials Science & Engineering
Northwestern University, Evanston, IL 60208-9990

Abstract

Spinel ($MgAl_2O_4$)(cubic) was compared with alumina (Al_2O_3)(hexagonal) as an oxide dispersoid in Al-3% Mg alloy. Selected because of its potential to improve the properties of dispersion strengthened Al, spinel has a lattice parameter almost twice that of Al, which might produce a good lattice match and low interfacial energy with Al in contrast to hexagonal Al_2O_3 where the interface is highly incoherent. Also, spinel is stable to 2000°C which minimizes diffusional deformation processes and adverse chemical reactions with the matrix that reduce the effectiveness of other particulates. Alloys of Al-Mg/spinel and AlMg/alumina were produced with 4 vol.% oxide by mechanical alloying. In a series of tensile creep tests performed at 410°C with stresses from 17 to 35 MPa, AlMg/spinel had a steady-state creep rate one order of magnitude smaller than AlMg/alumina at the same stress.

* Supported by the AFOSR under Grant No. AFOSR-85-0337

Introduction

Magnesium-aluminum spinel (cubic, nominal composition $MgAl_2O_4$) may be a better dispersoid for mechanically alloyed aluminum based oxide dispersion strengthened (ODS) metal matrix composites than hexagonal corundum (α-Al_2O_3) for several reasons. First, the lattice parameter of cubic spinel, a_o= 0.808 nm, is almost twice that of Al, a_o= 0.405 nm, and thus there is greater possibility of a coherent interface than with α-Al_2O_3, where the lower symmetry makes special orientation low interfacial energy relations between the dispersoid phase and matrix less likely. In the second place, spinel has a {111} cleavage habit while sapphire has no distinct cleavage habit [1]. For these reasons, reduction of particle size in the attritor and good distribution of the particles inside the metal matrix grains seem more likely in the case of the spinel. The latter process would be favored by a low energy interface. Furthermore, coherent-coplanar magnesium ferro-spinel ($MgFe_2O_4$) precipitates in cubic periclase (MgO) when they are very small are ductile at room temperature in that dislocations in MgO are able to cut through the precipitates[2]. Thus it is possible that small single crystal magnesium aluminum spinel particles dispersed in an Al alloy matrix may have limited plasticity, leading to improved ductility in the metal matrix composite Al base alloy.

Since MgO and Al_2O_3 react to form spinel with a lowering of free energy, a magnesium-aluminum alloy for the matrix seems appropriate. It should be pointed out that the melting point of spinel is slightly higher than that of corundum, 2100°C compared to 2015°C. At high temperatures spinel is stable over a wide range of Mg/Al ratios [3].

While α-Al_2O_3 has been widely investigated as a dispersoid for ODS aluminum alloys, the results have been somewhat disappointing due to low room temperature toughness [4]. Also, at least in some cases, the modulus of the composite falls below the rule of mixtures line indicating that the load is not being transferred across the interface [5].

For these reasons, a comparison of α-Al_2O_3 and spinel dispersions formed in an aluminum matrix by mechanical alloying using identical processing procedures is of interest. The results of a preliminary study with 4 vol.% spinel and 4 vol.% α-Al_2O_3 in an Al-3 wt.% Mg matrix are reported herein.

The usual method of mechanical alloying Al alloys has been to process the elemental metal powders in a high energy attritor using a surfactant to prevent excessive cold welding. This type of processing produces surface oxidation and thus introduces a fine dispersion of oxides into the final alloy. Breakdown of the surfactant leads to a dispersion of Al_4C_3 in the alloy [6]. For example, alloy IN9051 is mechanically alloyed Al-4 wt.% Mg containing aluminum and magnesium oxides from surface oxidation as well as Al_4C_3. The present goal was to develop a system which would allow mixing of dispersoid powders with the metal powders to obtain a high volume fraction of dispersoid in a useful alloy.

In the present research, since a mechanical attritor was not available and only small exploratory batches were desired, a laboratory vibratory mill with alumina cylinders was used for the mechanical alloying.

Materials Preparation

For the matrix, Al-3 wt.% Mg powder was supplied by the Alcoa Research Laboratory. The powder was prepared by rapid solidification of the alloy using a gas atomizer. The particle sizes ranged up to 100 μm but 90 wt.% were smaller than 45 μm and only 2% were larger than 75 μm. The α-Al_2O_3 and spinel powders were supplied by Baikowski International. The spinel was made by calcining co-precipitated aluminum and magnesium sulfate complexes. The α-alumina was prepared from aluminum. Analyses provided by the supplier

indicated that both ceramic powders were 99.9+% pure. According to the particle size analyses supplied by Baikowski International, the spinel powder particles were smaller than 12 μm (3 μm average size) and the α-alumina particles were smaller than 5 μm (0.5 μm average size). On average, the alumina powder particles were much smaller than the spinel particles. This characterization was verified by the SEM.

The mechanical alloying was carried out as follows. The desired amount of spinel or α-alumina was mixed with the Al-3% Mg powder to give 4 vol.% of dispersoid. The powders were coated with oleic acid to reduce cold welding [7] by stirring them in an oleic acid-acetone mixture and then evaporating the acetone. The treated powders contained 1 wt.% oleic acid. The coated powder mixture was sealed in a polyethylene jar containing 12 mm by 12 mm alumina grinding cylinders, and processed in a vibratory mill for one hour. Longer processing times led to excessive cold welding due to breakdown of the oleic acid.

The alloyed powders were consolidated in a two stage process. First the powders were cold pressed into billets 19 mm in diameter and 3.5 mm thick at 350 MPa pressure in a dual-action press. The cold-pressed billets were hot forged by heating them between steel plates to 710°C and pressing them at 16,000 Kg load between 25 mm dies heated to 140°C, the maximum operating temperature of the press. When heated to 710°C in the furnace, the billets had enough strength to allow transfer of the plate-billet assembly to the press. This procedure combines liquid metal infiltration with hot pressing.

The hot forged billets were ground to remove edge cracks giving pancakes 20 to 22 mm in diameter and 2 mm thick. The pancakes were then cold rolled in one direction with intermediate anneals for 5 min at 600°C to 0.8 mm thickness. The resulting strips were cut by electric discharge machining into tensile creep specimens with gage sections 5.0 mm long and 3.1 mm wide.

Microstructure of Cold-Rolled Strip

Optical microscopy (OM) showed that the cold rolled material consisted of pancake shaped grains, with the plane of the pancakes parallel to the rolling plane. In the spinel ODS Al alloy the grains appeared to be approximately 7 μm thick and 15 μm in diameter, while the grains of the α-alumina ODS Al alloy were approximately 7 μm thick and 30 μm in diameter. The grains were more or less equiaxed in the rolling plane but there were considerable variations in the dimensions. The grain dimensions ranged by a factor of two from the average.

The microstructures of the two ODS Al base alloys were examined by transmission electron microscopy. Thin foils parallel to the rolling plane were prepared by electrolytic thinning in a solution of 75 vol.% methanol and 25 vol.% nitric acid at -40°C using a 100 ma current and 50 to 60 volts.

In the case of the 4 vol.% spinel in the Al-3% Mg alloy matrix the spinel particles are well distributed inside many of the grains, as shown in the pair of bright and dark field micrographs of Fig. 1. The spinel particles were 30 to 150 nm in diameter. Since many particles of spinel were lit up in dark field centered around a spinel diffraction spot, an orientation relation between the spinel particles and the matrix is suggested; however, further research is needed to establish whether or not this is true since several spinel diffraction spots as well as matrix diffraction spots contributed to the image shown. Figure 1b, of course, does not show all of the spinel particles and the particles are rather difficult to see in Fig. 1a.

The grain size of the spinel ODS alloy seen by TEM is considerably smaller than that observed by the lower magnification OM. The grain boundaries seen optically no doubt are those delineated by oxide segregation.

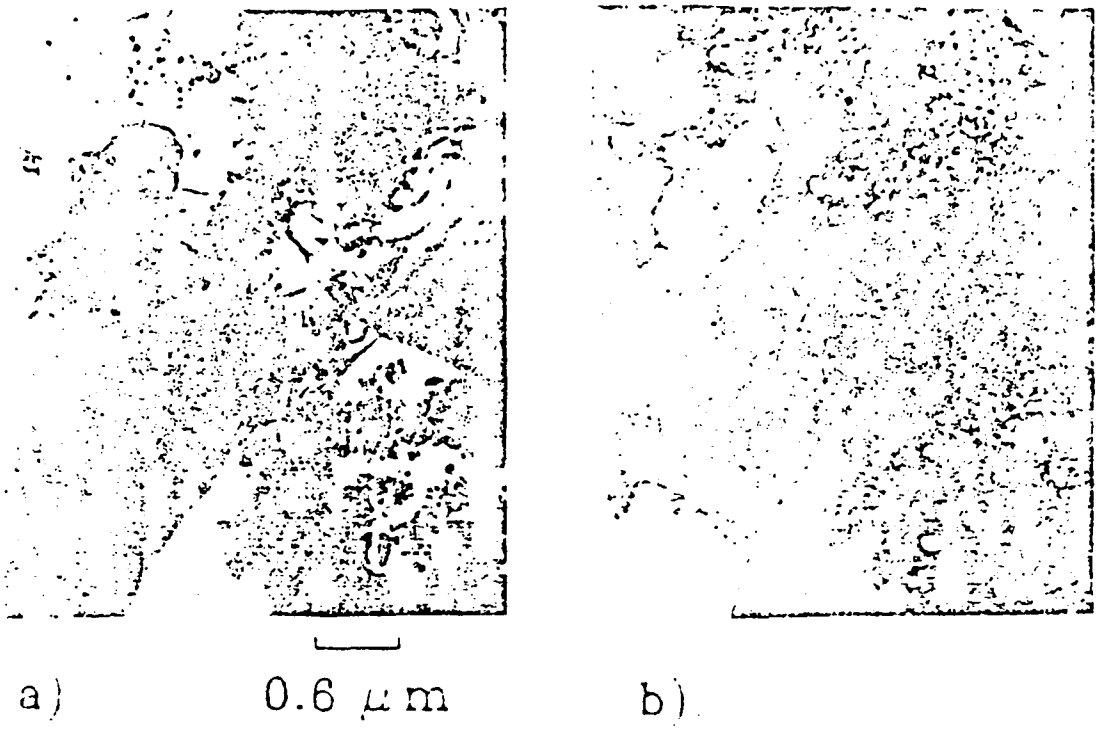

Figure 1 - Bright field (a) and dark field (b) TEM pair of 4 vol.% spinel in Al-3% Mg matrix after cold rolling and annealing. For dark field beam was centered on a spinel diffraction spot.

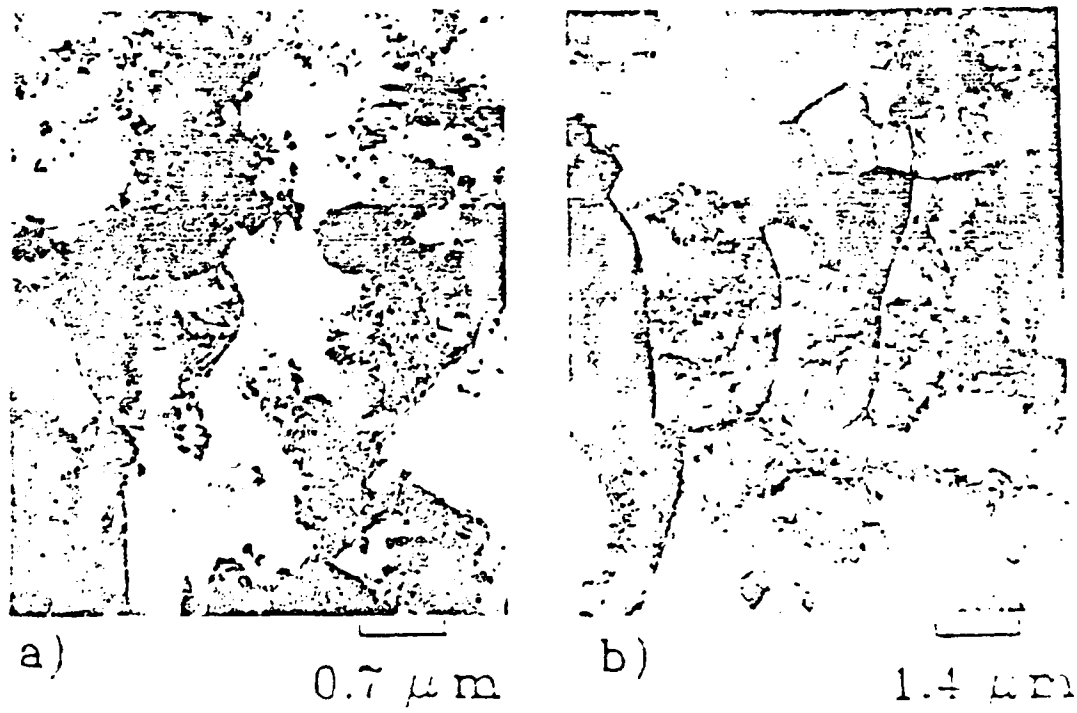

Figure 2 - Comparison of regions in 4 vol.% spinel in Al-3% Mg matrix containing many (a) and few (b) spinel particles. Bright field.

The grain boundaries in Fig. 1 show rather little oxide segregation. This observation is possibly also an indication that the interfaces formed inside the grains between the spinel and matrix alloy have a low energy.

The spinel particles are not distributed uniformly. Some grains seem to be devoid of dispersoids. These grains are larger. The spinel-rich areas have grain diameters in the foil plane of $\frac{1}{2}$ to 3 μm while the grains in the spinel poor regions are up to 10 μm across. Figure 2 shows lower magnification TEM micrographs, which give a better indication of the appearance of the grains. A much more uniform distribution of spinel particles, no doubt, could be achieved by better mechanical alloy processing.

The α-alumina particles were not nearly so well distributed in the matrix as were the spinel particles, as shown in Fig. 3. Because there were so many α-alumina diffraction spots, we were not able to form a useful dark field image. The α-alumina particles are larger than the spinel particles (150 to 300 nm across compared to 30 to 150 nm across) and considerably fewer of them were observed. Note that the original α-alumina powder was considerably finer than the spinel. Obviously the α-alumina particles were reduced less than the spinel by the mechanical alloying. The α-alumina ODS alloy also had the larger average grain size. The smallest grains were approximately 5 μm across compared to $\frac{1}{2}$ μm for the spinel ODS alloy.

As in the case of the spinel ODS alloy, the grain size of the α-alumina ODS alloy measured in the optical microscope was larger than that seen in the SEM, and again this discrepancy is attributed to regions of heavy oxide segregation making some of the grain boundaries visible in the OM. In fact, the first indication that the α-alumina particles did not disperse so well as the spinel came during the electro thinning of the foils for TEM observation. The α-alumina ODS alloys exhibited severe preferential etching along some grain boundaries making foils difficult to prepare.

The α-alumina particles have more random orientations than the spinel particles. This can be seen by comparing electron diffraction patterns, Fig. 4a and b. The diffraction rings are more complete for the α-alumina ODS alloy. Relatively fewer spots were seen with the spinel ODS alloy in spite of the fact that substantially more particles are present. Analyses of the diffraction patterns showed that indeed spinel and α-Al_2O_3 were present.

Uniaxial Tensile Properties

The uniaxial tensile properties at room temperature were determined using a screw driven Instron machine at a strain rate of 5×10^{-3}/sec. The principal difference between the uniaxial tensile properties of the two alloys at room temperature is the larger percent elongation to failure for the spinel ODS alloy, 15% compared to 8% for the α-alumina ODS alloy, as shown in Fig. 5. The combined results for two tests on each alloy are shown. The yield stress as determined from 1% offset from the "elastic" line for the spinel ODS alloy was lower than that of the α-alumina ODS alloy, 170 MPa compared to 190 MPa; however, the ultimate tensile strength of the former is larger due to its greater ductility. No significance is placed on the difference in slopes of the "elastic" lines since the elongation was obtained from the crosshead and not from an extensometer.

Creep Results

The creep tests were performed at 410°C in a dead-load creep apparatus. The specimens were enclosed in a fused quartz tube through which argon was flowing. Displacement was measured by an LVDT transducer on the lower loading arm of the creep apparatus outside the furnace. The specimen temperature was measured with a thermocouple next to the specimen and separate from the

control thermocouple.

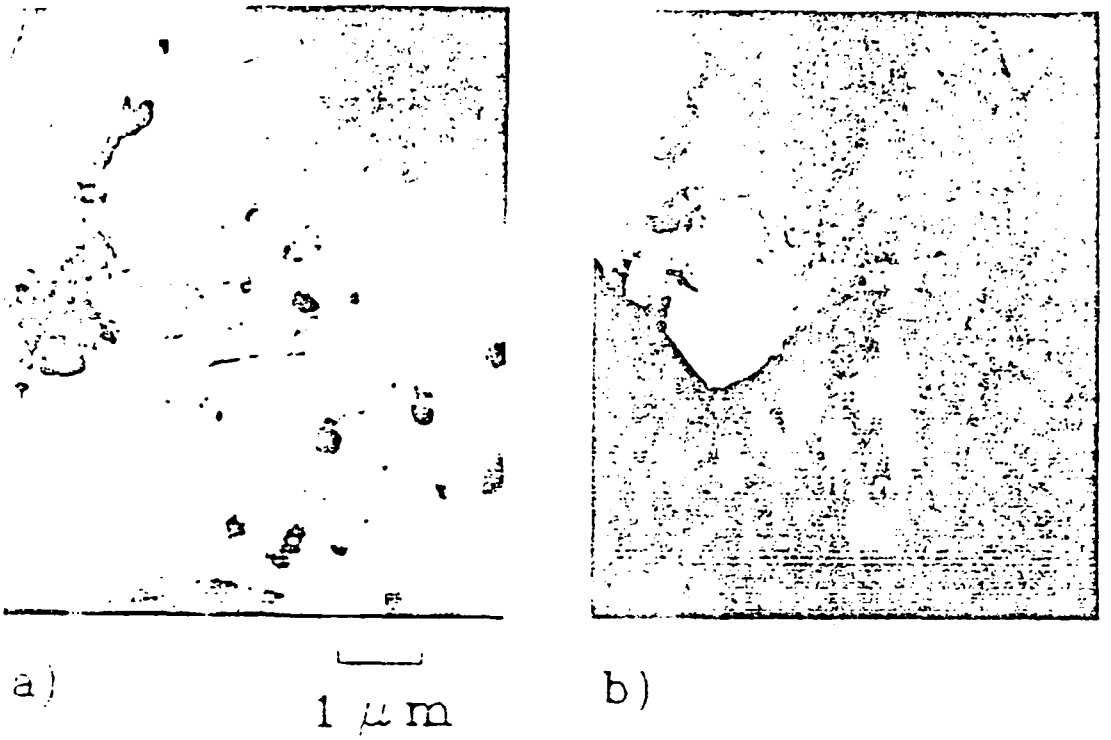

Figure 3 - Bright field (a) and dark field (b) TEM pair of 4 vol.% α-alumina in Al-3% Mg matrix after cold rolling and annealing. For dark field beam was centered on an α-alumina diffraction spot.

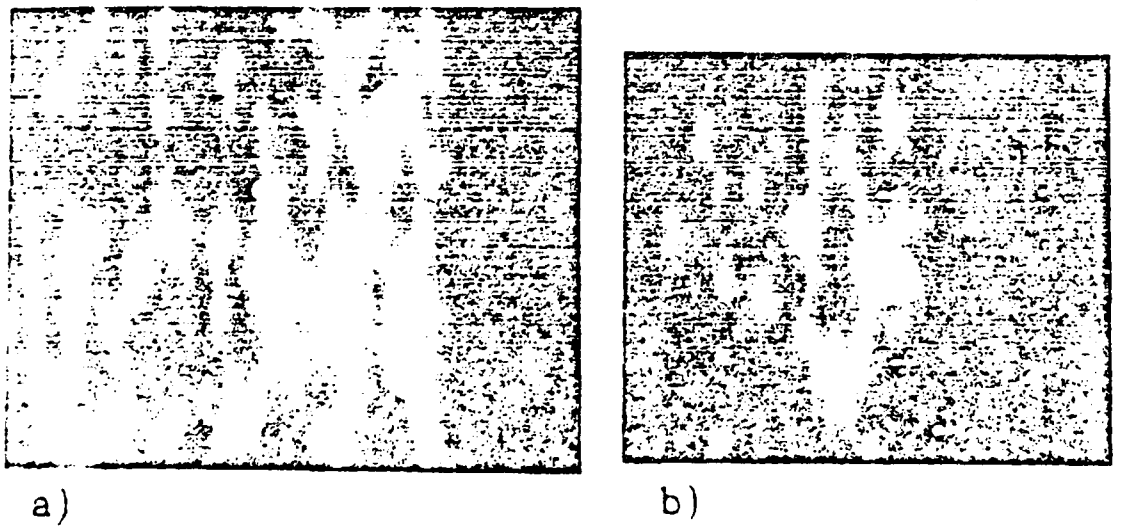

Figure 4 - Selected area electron diffraction patterns of 4 vol.% spinel (a) and 4 vol.% α-alumina (b) in Al-3% Mg matrix after cold rolling and annealing.

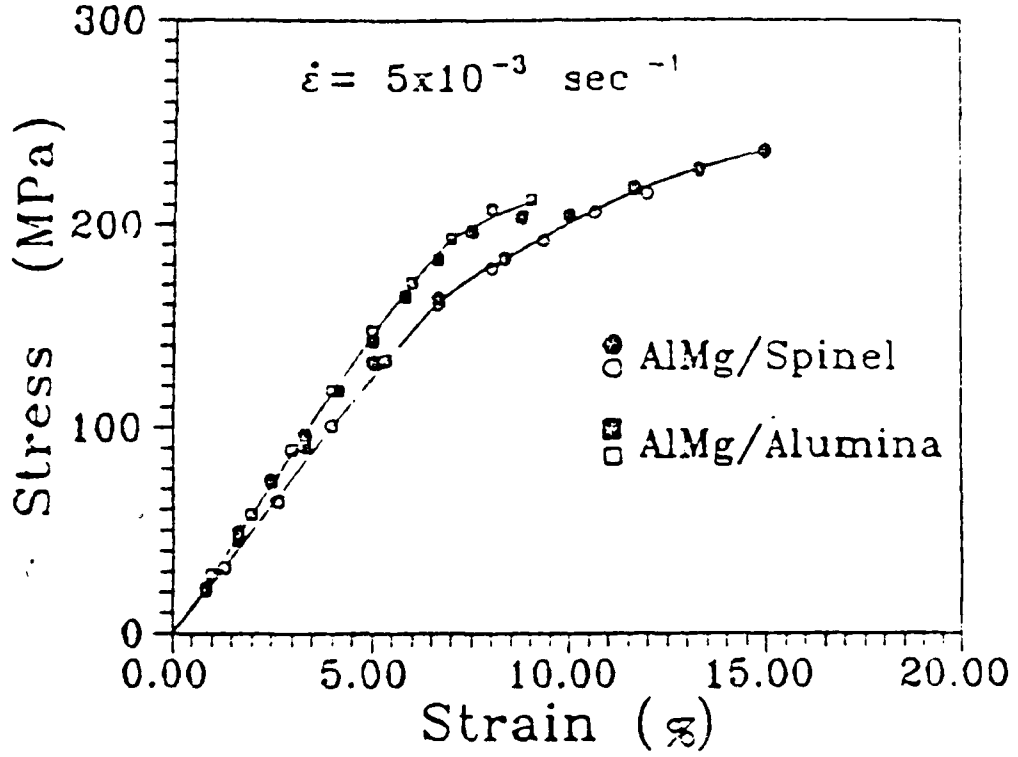

Figure 5 - Room temperature stress-strain curves of 4 vol.% spinel and 4 vol.% α-alumina in Al-3% Mg after cold rolling and annealing. Results of two tests for each are shown.

Tests were done at four nominal stress levels: 17, 22, 30 and 35 MPa. Some tests were run to failure. In others, the initial load was applied long enough to establish a steady state creep rate and then the stress was increased to obtain another data point. The steady state creep rates so obtained are given in Table I and plotted in Fig. 6.

Table I. Steady State Creep Rates at 410°C of 4 vol.% Spinel and 4 vol.% α-Al_2O_3 in Al-3% Mg Matrix

Stress, MPa	Spinel ODS Creep Strain Rate	α-Alumina ODS Creep Strain Rate
17	$<0.003 \times 10^{-6}$ sec^{-1}	1.34×10^{-6} sec^{-1}
22	2.03×10^{-6}	25.8×10^{-6}
30	105×10^{-6}	992×10^{-6}
35	624×10^{-6}	-
σ_t	14.2 MPa	8.7 MPa
m	5.7	7.0

The creep strain rate for the spinel ODS Al alloy was not measurable at 17 MPa stress and 410°C. No measurable strain was observed up to 430 hrs. Since the minimum measurable strain in the apparatus was 4×10^{-3}, the creep strain rate must have been less than 2.5×10^{-9}/sec. The α-alumina ODS Al alloy, on the other hand, had a measurable creep strain rate at 17 MPa. At 22 MPa the creep rate of the latter alloy was more than 10 times faster. The α-alumina ODS Al alloy broke on application of 35 MPa stress while the spinel ODS Al alloy had a measurable creep strain rate of 624×10^{-6}/sec.

The creep of ODS alloys is usually analyzed in terms of a threshold stress [8], as shown in Eq.(1):

$$\dot{\varepsilon} = A(\sigma - \sigma_t)^m \exp(-Q_c/RT) \qquad (1)$$

where A and m are constants and Q_c is an activation energy. At constant temperature

$$\ln \frac{\dot{\varepsilon}_1}{\dot{\varepsilon}_2} = m \ln \frac{(\sigma_1/\sigma_t - 1)}{(\sigma_2/\sigma_t - 1)} \qquad (2)$$

where the subscripts refer to different stress values. Thus m and σ_t may be determined from measurements of creep strain rates at three different stress levels. These values are also given in Table I. σ_t is higher for the spinel ODS Al alloy, as is obvious from inspection of $\dot{\varepsilon}$ vs σ data.

Discussion

The better creep properties of the spinel ODS Al alloy compared to those of the α-alumina ODS Al alloy are no doubt due to the better dispersion of particles which was achieved during the identical processing. Even though the volume fractions of dispersoids are the same, the spinel particle size is smaller than the α-alumina particle size and there are many more particles of the former thereby reducing the spacing between particles and consequently the creep rate. On the basis of the present data, it is not possible to definitely attribute the lower creep rates to better properties of spinel dispersoids beyond the fact that a finer dispersion of spinel

particles was achieved by the mechanical alloying processing used.

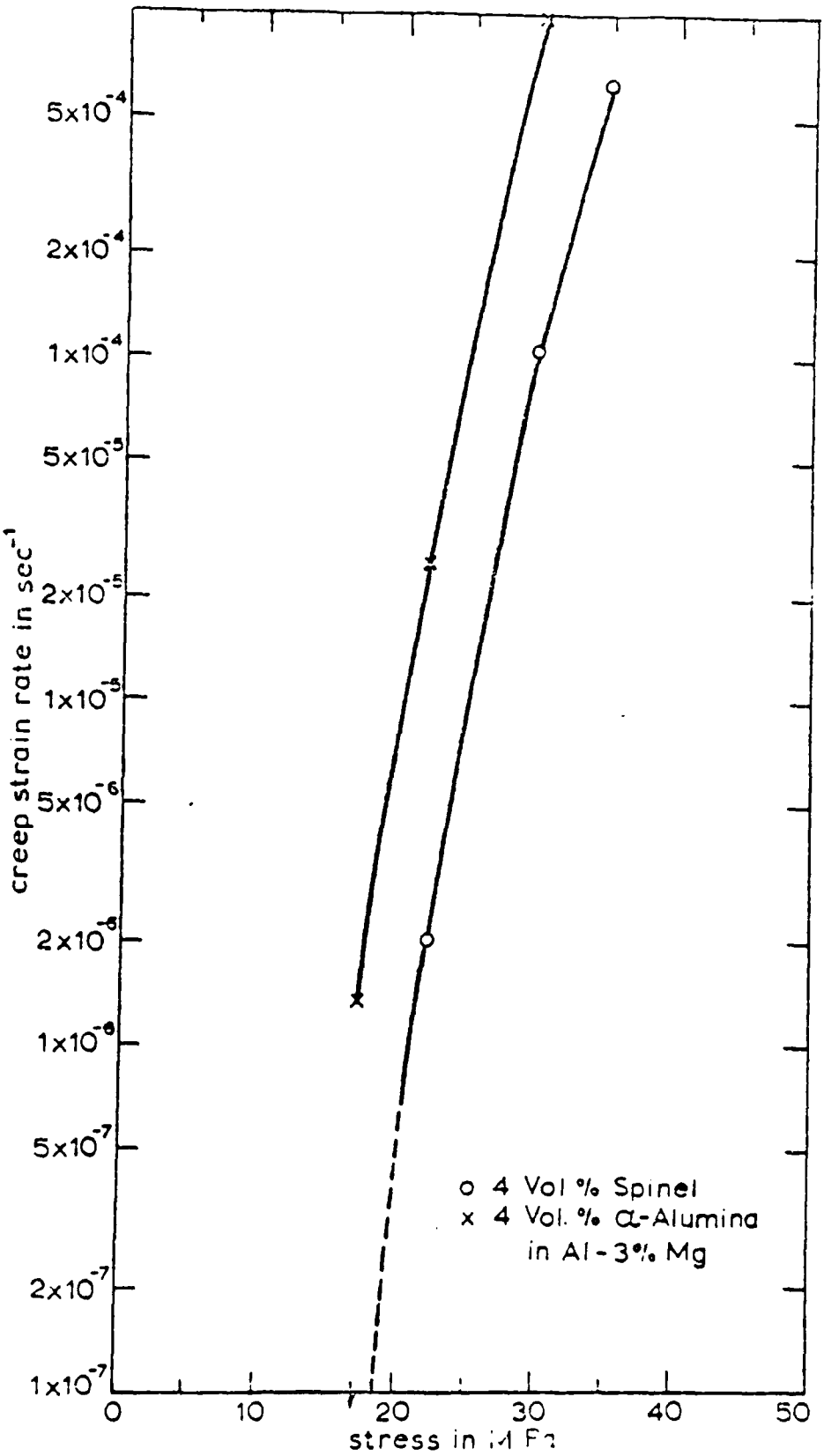

Figure 6 - Steady-state creep rates at 410°C of 4 vol.% spinel and 4 vol.% α-alumina in Al-3% Mg matrix.

Surprisingly, the α-alumina ODS Al alloy has the higher yield stress σ_y at room temperature in spite of the larger spacing, ℓ, between particles. An α-alumina particle must be a stronger obstacle to dislocation motion than a spinel particle. If the dislocations bypass the particles, one expects

$$\sigma_y \sim Gb/\ell \qquad (3)$$

and a stronger spinel composite since ℓ is smaller.

Therefore, it appears likely that dislocations have deformed the spinel particles to some extent. The greater ductility of the alloy containing spinel dispersoids may thus be partly due to the plasticity of the spinel. This is a very attractive possibility which is being explored.

At 410°C the spinel particles give the higher flow stress at a given strain rate, as seen from inspection of the creep data. It is again attractive to propose that dislocation cutting of the spinel occurs with the attendant formation of an anti-phase boundary. The energy required to achieve such boundaries in Ni_3Al type dispersoids, as is well-known, is the source of their remarkable creep strength and this possibility appears to exist for spinel in an Al matrix.

Al-4% Mg mechanically alloyed in a production type attritor and extruded has a higher yield stress at room temperature [9] and better creep resistance [7] at elevated temperatures than the present 4 vol.% spinel in Al-3% Mg matrix processed by the technique described herein. The combined volume fraction of oxide produced by surface oxidation and carbide in the former alloy is roughly 4 vol.% so the volume fractions of dispersoids are not too different in the two alloys. The oxides and carbides are well-dispersed and of quite small size when the alloy is produced with production type facilities. Also, Al_4C_3, as a dispersoid, is known to effectively strengthen Al. Of course, better distribution of spinel particles in the present alloy no doubt will result in much better properties; however, the major promise with spinel dispersoids is in obtaining an ODS Al base alloy with very much higher volume fractions of oxide dispersoids giving acceptable toughness at room temperature and the desired high strength and creep resistance at high temperatures needed for a useful high temperature alloy.

Conclusion

Although mechanical alloying for 60 min in a laboratory vibratory rod mill did not give a uniform distribution of either spinel or α-alumina dispersoid particles in an Al-3% Mg matrix, these preliminary results do show that, as predicted, spinel has a number of advantages over α-alumina for developing a suitable high temperature metal matrix Al base composite alloy. The mechanical alloying in the rod mill reduced the spinel particle size considerably more than the α-alumina particle size and the distribution of spinel particles achieved was much better with less tendency for grain boundary segregation. There was indication that the liquid metal infiltration consolidation method used resulted in an orientation relation between the spinel particles and the matrix. There was also indication that the spinel particles exhibited limited ductility during mechanical testing.

Research in progress with alloys with higher volume fractions of dispersoids is aimed toward verifying these preliminary conclusions and achieving better high temperature strength and creep resistance with good ductility.

Acknowledgment

The authors are pleased to acknowledge support of the Air Force Office of Scientific Research, USAF, under Grant No. AFOSR-83-0337.

References

1. E. S. Dana and W. E. Ford, A Textbook of Mineralogy, 4th edition (New York: John Wiley & Sons Inc., 1932) 481 and 485.

2. M. E. Fine, "Precipitation Strengthening of Some Metallic Oxides", Proceedings of International Conference on Strength of Metals and Alloys, Supplement to Trans. Japan Institute of Metals, 9 (1968) 527-531.

3. E. M. Levin et al., Phase Diagrams for Ceramists (Columbus, OH: The American Ceramic Society, 1964) Figs. 259 and 260.

4. J. Dinwoodie et al., "The Properties and Applications of Short Staple Alumina Fibre Reinforced Aluminum Alloys", Fifth International Conference on Composite Materials, ed. W. Harrington et al. (Warrendale, PA: The Metallurgical Society, 1985) 671-685.

5. M. E. Fine, "Elastic Moduli of Two Phase Aluminum Alloys", Scripta Metall., 15 (1981) 523-524.

6. J. S. Benjamin and M. J. Bomford, "Dispersion Strengthened Aluminum Made by Mechanical Alloying", Metall. Trans. A, 8A (1977) 1301-1305.

7. P. S. Gilman and W. D. Nix, "The Structure and Properties of Aluminum Alloys Produced by Mechanical Alloying: Powder Processing and Resultant Powder Structures", Metall. Trans. A, 12A (1981) 813-823.

8. L. M. Brown, "Creep of Metallic Composites Related to Deformation Mechanisms" in Fatigue and Creep of Composite Materials, ed. H. Lilholt and R. Talreda (Roskilde, Denmark: Risø Natl. Lab., 1982) 1-18.

9. Y-W. Kim and L. B. Bidwell, "Tensile Behavior of a Mechanically Alloyed Al-4.0 Mg Powder Alloy", Scripta Metall., 16 (1982) 799-802.

APPENDIX B

Submitted to Acta Metallurgica 8/20/83

Microstructural Evolution and Mechanical Properties of Rapidly Solidified Al-Zr-V Alloys at High Temperatures

Y. C. Chen*, M. E. Fine and J. R. Weertman, Department of Materials Science and Engineering, Northwestern University Evanston, IL 60208

I. Abstract

Aging studies of three melt spun Al-Zr-V alloys showed that precipitation of the metastable Ll_2 phase is favored over that of the equilibrium phases, $Al_{10}V$ and $Al_3Zr(DO_{23})$. The precipitation mechanism of the Ll_2 phase can be either continuous or discontinuous. The former is favored by decreasing the value of the Zr/V ratio in the Ll_2 phase precipitate or by increasing the aging temperature.

Coarsening of the spherical Ll_2-structured $Al_3(Zr_{.25}V_{.75})$ particles was studied at 425, 450 and 500°C. The activation energy calculated from the particle coarsening is close to that for diffusivity of Zr in the Al matrix, suggesting that volume diffusion of Zr is the rate controlling mechanism for the Ostwald ripening of the Ll_2-structured $Al_3(Zr_{.25}V_{.75})$.

The Ll_2 phase precipitate in extruded Al-1.13 Zr-1.82 V alloy grew slowly at 425°C, close to the rate measured in the melt spun ribbon. A high stress exponent in creep at 425°C, close to 14, is found for the extruded Al-1.13 Zr-1.82 V alloy. Dislocations cross-slip inside the Ll_2 phase particles from a {111} plane to a {100} plane during creep.

*Present address: Materials Research Laboratories, 195 Chung-Hsing Road, Chutung, Hsinchu, Taiwan 31015, R.O.C.

II. Introduction

By analogy with the γ' strengthened Ni-base superalloys, which are useful to three-quarters of the absolute melting temperature of Ni, development of a dispersion strengthened Al base alloy useful to approximately 425°C may be anticipated (1). To improve the strength of Al alloys at this high temperature, a microstructure containing a thermally stable and coarsening resistant dispersoid is required (2,3). According to particle coarsening theories, a dispersoid phase having low interfacial energy, low diffusivity D, and low solubility C_o at this temperature would be most coarsening resistant.

Zr has the smallest diffusion flux, i.e., DC_o, in Al among the transition metals (3). A coherent metastable phase, Al_3Zr, which is Ll_2-structured like the γ' (Ni_3Al) phase, and/or a semicoherent stable phase Al_3Zr which is tetragonal-structured may be present in the Al-Zr alloy system (4-6). They both are expected to have low interfacial energies, especially the former.

As found by Zedalis et al. (7) partial substitution of V for Zr in the precipitate not only increases the thermal stability of the metastable Ll_2 phase but also slows down the particle coarsening rate at 425°C. In an Al-5 vol. % $Al_3(Zr_{.25}V_{.75})$ alloy, a very slow growth rate of the Ll_2 phase precipitate was measured at 425°C (8). Thus Al-Zr-V base alloys are promising for use at high temperatures.

In the present study, three Al-Zr-V alloys with different Zr/V ratios prepared by melt spinning were used to study the thermal stability of the metastable Ll_2 phase with respect to both phase change and Ostwald ripening. Mechanical properties of extrusions made from the three melt spun ribbons were also evaluated at 425°C.

III. Experimental Procedures

Based on the assumption that the solid solubilities of both Zr and V in aluminum are 0.1 wt% at 425°C, approximately the solubility of these elements in the binary Al alloys, three Al-Zr-V alloys designed to contain 5 vol% $L1_2$-structured $Al_3(Zr_xV_{1-x})$ were prepared by melt spinning. The values of x were 0.75, 0.5 and 0.25 and the alloys were designated as alloys 2, 3, and 4, respectively. The nominal compositions of these three alloys are given in Table 1. Extruded bars having dimensions of 6.4x14 mm^2 were made from these ribbons through vacuum hot degassing, hot pressing and hot extrusion. The process details were described elsewhere (9).

The microstructures of the melt spun ribbons and extruded bars were examined by optical and electron microscopy. The specimens for optical microscopy were prepared by electropolishing and etching in Keller's reagent. TEM foils were prepared in a double jet polishing apparatus by employing a solution of 25 vol.% nitric acid in methanol. The temperature of the electrolyte was kept between -40 to -60°C and a current of 100 mA was applied. For making thin foils from the melt spun ribbons, mechanical polishing with 600-grit abrasive paper was done prior to electro-polishing to remove the surface roughness and contamination. Some specimens were prepared specifically to examine the microstructures near both surfaces of the ribbons. These specimens were selectively polished on one surface with the other one protected with lacquer. After electro-polishing, the lacquer was dissolved in acetone. Sometimes ion milling was applied at 2 mA and 4 kV for half an hour at a grazing angle of 15° to remove surface contamination.

Extracted second phase particles were obtained by electrolytic dissolution of the Al matrix in an electrolyte, suggested by Cocks et al.(10), containing 60 g benzoic acid, 15 g 8-hydroxyquinoline, 60 ml chloroform and 160 ml methanol.

The particle sizes of the Ll_2 precipitates were measured from the TEM negatives taken by the central dark field (DF) technique using superlattice reflection spots. More than 400 particles were measured for each determination of average particle radius. The precipitate free zone (PFZ) widths were measured with the beam direction lying in the grain boundary plane.

Creep tests were conducted at $425\pm2^{o}C$ on a dead load creep machine. Strain was monitored with a calibrated linear variable differential transducer. Tensile tests were carried out on an MTS machine at $425^{o}C$. Both kinds of test were done in an Ar atmosphere. The specimens (S1 and S2) are shown in Figure 1.

IV. Results

1. Microstructures and phase transformations in the melt spun ribbons

The melt spun ribbons, approximately 20-60 μm thick and 2-3 mm wide, occasionally had small globules of previously molten metal stuck on them. All the investigated specimens were chosen to avoid these regions. The optical microscopy observations disclosed that alloy 4, which contains the most V, shows a more sluggish response to etching than alloys 2 and 3. The former exhibits a featureless appearance until the etching time is longer than 4 minutes, while two minutes of etching revealed the structure of alloys 2 and 3. The microstructure of alloy 4 varied slightly from place to place, depending upon the contact of the ribbon with the chilled Cu wheel. As shown in Figure 2a, columnar grains are observed in the ribbon where the chill surface is flat. However in some areas where the chill surface is uneven (Figure 2b) a dark-etching phase region is present near the free surface of the ribbon which was in contact with the atmosphere during the melt spinning. A lower cooling rate is associated with such an uneven contact surface.

TEM selected area diffraction (SAD) (11) showed that the second phase particles present near the the free surface of alloy 4 have the structure of $Al_{10}V$. No $Al_{10}V$ phase particles were found in the as-melt spun ribbons of alloys 2 or 3. Typical microstructures from the areas close to the middle of as-melt spun ribbons of alloys 2, 3 and 4 are shown in Figure 3. In alloys 2 and 3, which have higher Zr/V ratios, cellular fan shaped precipitates form inside some grains (Figures 3a and 3b). The TEM selected area diffraction patterns in the inset of Figure 3b shows that these cellular precipitates have the Ll_2 type structure. The grain boundaries are rather irregular and island grains surrounded by other grains are often observed in these two alloys. In alloy 4, no precipitates were noted inside the grains and the grain boundaries

are more regular, as seen in Figure 3c. Along the grain boundaries, some small second phase particles, approximately 0.1 μm in size, are present. TEM selected area diffraction from the larger of these particles proved that they also have the structure of $Al_{10}V$. This grain boundary precipitate is likely to be the source of the etch pits at grain boundaries seen in Figure 2a.

In Figure 3a and Figure 3b, a second kind of precipitate is seen in addition to the cellular Ll_2 phase. In the TEM dark field micrographs of Figures 4a and 4b, this phase is clearly distinguishable from the cellular Ll_2 precipitates. It has not been previously reported in either the binary Al-Zr, Al-V or ternary Al-Zr-V systems and was named "Q" phase. Since all the "Q" phase particles in one grain always light up at the same time with one operating superlattice reflection, they must have the same crystallographic orientation, i.e., the "Q" phase is coherent with the matrix.

Analyses of electron diffraction patterns of the "Q" phase show it to be simple cubic with a lattice constant of 0.406 nm (11). This value is quite close to the lattice constant of Al, 0.405 nm. A cube/cube orientation relationship with the matrix like that existing between the Ll_2 phase and the Al matrix does not exist for the "Q" phase (11).

Aging at 500°C for 1 hour did not cause the microstructures of alloy 2 and 3 ribbons (11) to change much except that equilibrium phase particles, $Al_{10}V$ and DO_{23}-structured Al_3Zr, formed on the grain boundaries. In alloy 4 after aging at 350°C for 3 hours, the cellular Ll_2 phase had begun to form from the grain boundaries as shown in Figure 5. The cellular Ll_2 phase has been suggested by Nes and Billdal (12) to form by discontinuous precipitation resulting from grain boundary movement. This is confirmed by the presence of the original traces of the grain boundaries, indicated by arrows in Figure 5, which are left behind the cellular decomposition.

In other areas, selected area electron diffraction indicates that after 3 hours at 350°C the matrix in alloy 4 is still free of any precipitate. During further aging to 30 hours at the same temperature (11), small spherical $L1_2$ phase particles form by continuous precipitation inside all the previously undecomposed grains. The fraction of the cellular $L1_2$ precipitate decreases with increase of the aging temperature (7). On aging at 600°C, cellular precipitates are not found at all.

During aging of Alloy 4 ribbon, the equilibrium phases $Al_{10}V$ and DO_{23}-structured Al_3Zr precipitate on the grain boundaries, leading to the formation of $L1_2$ precipitate free zones (PFZs). Both grain boundary precipitate size and PFZ width increase with aging time (8, 13). Most of the grain boundary precipitates seen in alloy 4 ribbon have the structure of $Al_{10}V$. A high resolution TEM (HRTEM) micrograph, Figure 6, reveals that microtwins and stacking faults are present in the $Al_{10}V$ phase particles. The existence of twins is also indicated by the twin spots shown in the electron diffraction pattern (inset in Figure 6). Using the energy dispersive X-ray spectrometry (EDS) attachment in an STEM, the average composition of extracted "$Al_{10}V$" phase particles was analyzed to be approximately 11 at.% V, and 1 at.% Zr, balance Al. A standardless analysis technique and thin film approximation were used. For simplicity, the nominal designation $Al_{10}V$ is used for this ternary grain boundary precipitate throughout this paper.

After aging at 600°C for 1.5 hours, the $L1_2$ phase is still ordered. This is determined by electron diffraction and the HRTEM micrograph shown in Figure 7, where each white spot corresponds to the image from the projection of Al atoms stacked along the [110] direction. A perfect lattice match between the $L1_2$ particle and the Al matrix, and a stepped interface are seen in this figure.

The growth kinetics of the spherical Ll_2 particles in alloy 4 ribbons were studied at 425, 450 and 500°C. For the coarsening studies at 425 and 450°C, a preaging at 500°C for 2.5 hours was carried out in order to largely suppress the cellular Ll_2 phase. The detailed coarsening results at 425°C have been reported previously (8). Figure 8 shows the coarsening kinetics of the Ll_2 particles at these three temperatures, where the cube of the average particle radius, $\bar{r}$, is plotted against aging time. The linear correlation coefficient, R, and the slope for each best fitting line are given in Table 2.

Typical Ll_2 particles in alloy 4 ribbon after aging at 500°C for 20 and 206 hours are shown in Figures 9a and 9b, respectively. A planar fault exists inside many Ll_2 phase particles as seen in Figure 9b. These planar faults are always parallel to the {100} planes of the Ll_2 phase. HRTEM study indicated these planar faults to be antiphase boundaries (APBs) which are associated with displacements of a/2<110> on {100} planes, where a is the lattice contant of the Ll_2 phase (11). In an Ll_2 precipitate containing an APB, preferential growth along the APB is noted. This causes some Ll_2 precipitates to appear as rounded parallelepipeds rather than rounded cuboids.

2. Microstructures and Mechanical Properties of Extruded Alloys

The microstructures of the three alloys after consolidation and extrusion look similar to one another in the optical microscope. Some coarse second phase particles are observed, as shown in Figure 10. The size of these particles is approximately 1 μm. Presumably, these regions came from the previously mentioned globules of molten metal which splashed onto already solidified ribbons. More of these coarse second phase particles were found in extruded alloy 2 than in the other two alloys. TEM observation reveals that the grain sizes, or subgrain sizes, in all three alloys were reduced to around

0.5 μm after extrusion, as shown in Figure 11. Basically, alloys 2 and 3 have microstructures similar to those in the melt spun ribbons but they show broken cellular Ll_2 phase regions resulting from the heavy plastic deformation.

In extruded alloy 4, all the Ll_2 phase particles are spherical. No cellular Ll_2 phase is observed. The size of the Ll_2 particles is still quite small but the number of particles in the extruded material appears to be somewhat less than in the melt spun ribbon. In some grains, stable tetragonal Al_3Zr particles are also found. The growth of the spherical Ll_2 phase in extruded alloy 4 is slow at 425°C. A volumetric coarsening rate of 1.1×10^{-28} m^3/hr was determined, which is close to that measured in the melt spun ribbon at the same temperature, 1.0×10^{-28} m^3/hr.

Tensile properties at 425°C for extruded alloys 2 and 4 are given in Table 3. Different strain rates as indicated were employed to acquire yield stress and tensile strength in accordance with ASTM E 151-64. Each data set was obtained from the average of two tests. At 425°C alloy 2 has a lower yield strength than alloy 4, 13.8 MPa compared to 42.7 MPa. The elongations obtained at 425°C for both alloys are less than those from the room temperature tests, which were around 30% (9). This drop in ductility with increasing temperature, at least in part, is due to thin specimens (S1, Figure 1a) used for the tensile tests at 425°C. Necking is expected to occur earlier in thin specimens, reducing the total elongation.

Creep tests were undertaken at 425°C with an initial stress of 17 MPa. Typical creep curves for the three extruded alloys, using the S1 specimen geometry (Figure 1a), are shown in Figure 12. As seen, alloy 2 creeps much faster than alloys 3 and 4 although its microstructure is similar to that of alloy 3 after extrusion. Alloy 4 exhibits the best creep resistance. The fracture surfaces, which are believed to relate to the fracture mode, are also

different for alloy 2 compared to alloys 3 and 4. Figure 13 is a fractograph from the crept alloy 2. A dimple structure and a large cross section reduction are seen over the whole fracture surface. The large reduction in area indicates that alloy 2 behaves in a ductile manner during fracture. In alloys 3 and 4, two distinct features are observed on the fracture surface, Figure 14a. The crack began from the left-hand edge in an intergranular fracture mode as shown in Figure 14b under a higher magnification. As noted in Figure 14a, the reduction of the cross section on the left-hand side is small. However, on the right-hand side, a dimple structure associated with a large cross section reduction similar to Figure 13 is present.

In extruded alloy 4, spherical Ll_2 phase particles were sheared by dislocations which results in formation of planar faults inside the Ll_2 phase particles. As seen in Figure 15, these planar faults lie on {100} planes. It implies that dislocations cross-slipped inside the Ll_2 phase particles from {111} planes to {100} planes during creep. Occasionally, a pileup of dislocations is observed within a PFZ, suggesting that the localization of plastic deformation may occur in this soft region.

The steady state creep rate at 425°C was studied as a function of creep stress for extruded alloy 4 using the thicker S2 specimen configuration (Fig. 1b). A partial correction for the change in stress caused by the drop in cross sectional area in the course of a creep test was made from the relationship

$$\sigma = \sigma_i / (1 - \epsilon) \qquad (1)$$

where σ_i is the initial stress, σ is the corrected stress and ϵ is the strain at the beginning of steady state creep. The total change in area in the course of a creep test was only 1 or 2 percent. The normalized steady state creep rate vs normalized stress σ_i is plotted in Figure 16. The normalized

creep rate is defined as $\dot{\epsilon}_s kT/DGb$ and the creep stress is normalized by dividing it by the shear modulus G. The stress exponent n ($\dot{\epsilon}_s \sim \sigma^n$) is found to be close to 14.

$\dot{\epsilon}_s$ - Epsilon dot, lc s

σ^n - sigma, lc n

V. Discussion

1. Microstructure of the rapidly solidified Al-Zr-V alloys as function of composition

Dissolved zirconium increases the lattice constant of the Al matrix. However, vanadium behaves in the opposite sense. The values by which the lattice constant of the Al solid solution changes on dissolution of 1 wt.% of Zr and V are +0.0005 nm and -0.00033 nm, respectively (14-16). Based on these values and Vegard's law, the changes of the lattice constant, Δa, for the three Al-Zr-V alloys are calculated and listed in Table 4. It is assumed that each alloy is in a supersaturated solid solution state. As can be seen, alloys 2 and 3 have larger lattice expansions over unalloyed Al than alloy 4. According to Hume Rothery's rule, supersaturated alloys 2 and 3 are expected to be more unstable than the supersaturated alloy 4. This may contribute to the different as-melt spun microstructures seen in the three alloys, with precipitation occurring in alloys 2 and 3 but not in alloy 4 (Figure 3). The lower liquidus temperature of alloy 4 due to a lower Zr content compared with alloys 2 and 3 may also play a role in suppressing precipitation in this alloy during solidification by lowering the temperature range where precipitation may occur.

The precipitation characteristics in Al-Zr-V alloys basically are similar to those in binary Al-Zr alloys, except near grain boundaries. The metastable Ll_2-structured $Al_3(Zr,V)$ phase may form in cellular or spherical morphology depending on whether the precipitation process is discontinuous or continuous. In general, the kinetics of discontinuous precipitation is controlled by grain

boundary diffusion (12). It is expected that at low aging temperatures discontinuous precipitation is kinetically faster than continuous precipitation. Consequently, Ll_2 phase in cellular morphology precipitates out first and becomes dominant in alloy 4 ribbon when aged at 350°C. With increased aging temperature, matrix diffusion becomes more competitive with grain boundary diffusion. This leads to the result that the spherical Ll_2 phase is dominant in alloy 4 ribbon after aging at 500°C or higher. As a result, the cellular Ll_2 phase may be suppressed by an initial treatment at a higher aging temperature as found by Zedalis in a dilute Al-Zr-V alloy (7).

Alloy composition may also play a role in the precipitation kinetics of the Ll_2 phase. In Al-5 vol.% $Al_3(Zr_{.125}V_{.875})$ alloy which was splat quenched and has the V/Zr ratio close to 7, the cellular Ll_2 precipitation is completely suppressed when aging is carried out at 500°C (1). However, to suppress the cellular Ll_2 precipitation completely in alloy 4 with a V/Zr ratio close to 3, aging must be done at a higher temperature, 600°C (8). As for alloys 2 and 3 which have V/Zr ratios close to 0.3 and 1, respectively, the cellular Ll_2 phase forms immediately after solidification. This indicates that a high V/Zr ratio promotes the continuous precipitation over the discontinuous precipitation mode.

As shown by Zedalis et al. (7), an Ll_2-structured $Al_3(Zr_xV_{1-x})$ phase with a high V content, i.e., small x, has better lattice matching with the Al matrix than does a precipitate with low V content. Thus, the effect of the V/Zr ratio on the continuous precipitation of the Ll_2 phase might be explained by a lower nucleation energy barrier due to a better lattice matching allowing easier homogeneous nucleation.

2. Coarsening kinetics of the spherical Ll_2 phase in the melt spun ribbon of alloy 4

The growth behavior of the Ll_2 particles at 425, 450 and 500°C shows good agreement with the $\bar{r}^3$ vs t relationship, $\bar{r}^3 - \bar{r}_o^3 = Kt$, which suggests that an LSW-type volume diffusion controlling process (2) is the coarsening mechanism. Here $\bar{r}$ is the average particle radius after aging for time t and $\bar{r}_o$ is an integration constant. If the effect of the precipitate volume fraction on Ostwald ripening is taken into account, the coarsening rate constant K for an alloy containing 5 vol.% of precipitates is given by (17)

$$K = \frac{12\,\gamma\, D V_m^2 C_o}{9RT} \qquad (3)$$

where γ is the interface energy, V_m is the molar volume of the precipitate, and R is the gas constant. This equation has been used by others to determine the activation energy of diffusivity of solute in the matrix from the experimental coarsening results (18-20). After rearrangement, equation (3) becomes

$$\mathrm{Ln}\ (KT/C_o) = \ln A - Q/RT \qquad (4)$$

where A is given by

$$A = \frac{12\,\gamma\, D_o V_m^2}{9R} \qquad (5)$$

and Q is the activation energy of diffusivity for the coarsening rate-controlling element in the matrix. The value of A is a slowly varying function of temperature and usually may be regarded as a constant over a small temperature range. Therefore, the value of Q can be experimentally determined from a plot of $\ln(KT/C_o)$ versus the reciprocal of temperature.

In the present alloy, neither the concentration C_o' of V or of Zr in the solid solution Al matrix in equilibrium with the metastable Ll_2 phase is accurately known. Here C_o' instead of C_o is used since the Ll_2 phase is a metastable phase. For a first order approximation, C_o' is assumed to be constant in the temperature range from 425 to 500°C. From the plot of ln(KT) versus 1/T shown in Figure 17, Q is calculated to be 294 KJ/mole. This value is closer to the activation energy for diffusion of Zr in Al, 242 KJ/mole, than the value for V, 82 KJ/mole (3,21). Consequently, the volume diffusion of Zr is most likely the rate controlling process for the Ostwald ripening of the Ll_2-structured $Al_3(Zr_{.25}V_{.75})$, as expected originally.

In binary Al-Zr alloys, the solvus line of the stable phase $Al_3Zr(DO_{23})$, C_o, can be expressed by the following equation, in wt%, (22)

$$C_o = 1180 \exp(-64.96 \text{ KJ/RT}) \qquad (6)$$

If it is assumed that the Zr concentration of the Al matrix in equilibrium with the metastable Ll_2 phase, C_o', does not change much from C_o, then a better calculation for Q can be obtained by considering the temperature dependence of C_o' from equation (6). The final result for Q is 229 KJ/mole. This value agrees even better with the activation energy of diffusivity for Zr in Al measured in a binary Al-Zr alloy (21). It was also found that the growth kinetics of the PFZ at 425°C in alloy 4 ribbon is controlled by the volume diffusion of Zr in the Al matrix (13).

3. Mechanical properties of extruded materials at elevated temperature

The poor creep resistance of extruded alloy 2 (Figure 12) is related to its low yield stress, 14 MPa at 425°C, which is lower than the creep stress, 17 MPa. The plastic tearing seen in the alloy 2 fracture surface after failure by

creep confirms this. But it is interesting to know why this alloy possesses a low strength compared with the other two extruded Al-Zr-V alloys since they all contain around 5 vol.% of precipitates.

TEM investigation disclosed that in alloy 2 slightly more Ll_2 phase particles transformed to the equilibrium phases compared with that in the other two extruded alloys after an annealing of 1 hour at 425°C. This difference was not seen in the melt spun ribbons of the three alloys. Thus it indicates that after hot extrusion the thermal stability of the Ll_2-structured $Al_3(Zr_{.75}V_{.25})$, which has a high Zr/V ratio, is less than that of the Ll_2 precipitates with lower Zr/V ratio. Another factor contributing to the weakness of alloy 2 at 425°C is its structural inhomogeneity (Figure 10). The regions with coarse second phase particles are not expected to contribute any significant strength to the alloy.

From the fracture-mechanism maps for a commercial pure Al (23), the fracture mode at 425°C with a creep stress of 17 MPa is located in the transgranular fracture regime. However, it is expected (23) that intergranular fracture in creep is more prominent in a particle hardened alloy. This is confirmed by the present result. Intergranular fracture was seen in alloys 3 and 4. Localization of plastic deformation along the PFZ's, which are softer than the matrix with its strengthening Ll_2 phase particles, and sliding of the grain boundaries or subgrain boundaries are assumed to be the mechanisms for the intergranular fracture seen in these two alloys.

In Figure 14a the creep crack grew by intergranular fracture to the middle of the cross section and then changed to transgranular. As the crack deepens the creep stress increases because of the reduction in cross section, becoming 34 MPa when the cross section is one half of its original value.

This value is becoming comparable to the 0.2% offset yield stress, 43 MPa, of alloy 4 at 425°C. Accordingly a transition is expected from an intergranular to a transgranular fracture exhibiting a dimple structure and a large reduction in cross section.

The creep theories for particle strengthened alloys proposed currently in the literature (24-28) suggest that processes occurring in the matrix are rate controlling for the creep of particle strengthened alloys. Thus, the creep rate equation for particle strengthened alloys is expected to be in the same form as that for the matrix material if an effective creep stress σ_{eff} equal to $\sigma - \sigma_o$ instead of actual stress σ is used, where σ_o is the friction stress or the threshold stress.

An empirical equation for the steady state creep rate $\dot{\epsilon}_s$ of pure Al in the power law regime is given by (29)

$$\dot{\epsilon}_s = A_D \, (DGb/kT) \, (\sigma/G)^{4.4} \qquad (7)$$

where A_D is an empirical constant equal to 3.4×10^6 for Al. Therefore the creep rate obtained in extruded alloy 4 may be expected to fit the following equation

$$\dot{\epsilon}_s = A_D \frac{DGb}{kT} \left(\frac{\sigma - \sigma_o}{G} \right)^{4.4} \qquad (8)$$

By linear regression, the value of σ_o is calculated to be 14.2 MPa.

For the case in which the structure of the alloy is invariant, i.e., the subgrain size or barrier distance for dislocations does not change during creep, Lin and Sherby (27), and Sherby et al., (30) proposed a semi-empirical

equation for the creep rate of particle strengthened alloys

$$\dot{\epsilon}_s = \varkappa \left(\frac{\lambda}{b}\right)^3 \frac{D_{eff}}{b^2} \left(\frac{\sigma - \sigma_{th}}{E}\right)^8 \qquad (9)$$

where λ is the subgrain size or barrier distance for dislocations, D_{eff} is the effective diffusion coefficient, E is Young's modulus, b is the Burgers vector, σ_{th} is a threshold stress and $\varkappa$ is a material constant equal to about 10^9 for high stacking fault energy materials. Since the subgrains in alloy 4 are usually pinned by the subgrain boundary precipitates, a constant subgrain structure during creep may be expected in this alloy. Therefore, it is of interest to compare the present creep results with those predicted by equation (9). Based on this equation, a threshold stress of 8.7 MPa is obtained from the linear regression.

A plot of creep rate versus creep stress for the data obtained from alloy 4 is compared with the curves predicted by equations (8) and (9) in Figure 18. The data fall between the predicted values. While the general trends are similar, the actual strain rates are off by several orders of magnitude from the predicted curves. A somewhat higher creep rate in alloy 4 compared with that from equation (8) might be caused by the localization of deformation within the PFZ's.

VI. Conclusions

1. In rapidly solidified Al-5 vol.% $Al_3(Zr_xV_{1-x})$ alloys, the metastable Ll_2 phase precipitates initially instead of the equilibrium phases, $Al_{10}V$ and $Al_3Zr(DO_{23})$. The precipitation mechanism of the Ll_2 phase depends on alloy composition and aging temperature. In the alloys with a Zr/V ratio equal to 3 or 1, a cellular Ll_2 phase forms by discontinuous precipitation immediately after solidification. However, supersaturated solid solutions are obtained in the alloys with a Zr/V ratio equal to 1/3.

2. In a supersaturated Al-1.13 Zr-1.82 V alloy, cellular Ll_2 is dominant when aging is carried out at low temperatures, because grain boundary diffusion is faster than matrix diffusion. Spherical Ll_2 particles become favored when aging is done at higher temperatures.

3. A good linear relationship between the cube of the average particle radius and aging time is obtained for the Ll_2-structured $Al_3(Zr_{.25}V_{.75})$ precipitate aged at 425, 450 or 500°C. Volume diffusion of Zr in the Al matrix appears to be the rate controlling mechanism for coarsening. The coarsening rate of the Ll_2 phase precipitate at 425°C is $1.1\times10^{-28}m^3/hr$.

4. In the extruded Al-5 vol.% $Al_3(Zr_{.25}V_{.75})$ alloy, Ll_2 phase precipitates were sheared by dislocations on {100} planes during creep, suggesting that cross slip of dislocations from a {111} plane to a {100} plane occurred inside the Ll_2 phase precipitate.

5. Extruded Al-5 vol.% $Al_3(Zr_{.25}V_{.75})$ alloy shows a high stress exponent, close to 14. With introduction of a threshold stress of 14.2 MPa, the stress exponent can be reduced to the value obtained for pure Al, 4.4. However, when an effective stress instead of the actual stress is considered, the experimental creep rates of alloy 4 are much faster than those predicted by Dorn's creep equation for pure Al.

Acknowledgements

This research was supported by the Air Force Office of Scientific Research Grant No. AFOSR-85-0337 under the direction of Dr. Alan Rosenstein. The authors are particularly grateful to R.E. Lewis and D.D. Crooks, Lockheed Missiles and Space Co., for preparing the materials. The use of the facilities of Northwestern University's Materials Research Center sponsored under the NSF-MRL Grant No. DMR8520280 is greatly appreciated. The authors would like to thank Professor L.D. Marks and Dr. J.P. Zhang of Northwestern University for assistance with the high resolution electron microscope.

REFERENCES

1. L. Angers, Y. Chen, M. R. Fine, J. R. Weertman and M. S. Zedalis, "Rational Design of High Temperature Aluminum Alloys" in Aluminum Alovs--Physical and Mechanical Properties, vol. I, E. A. Starke, Jr. and T. H. Sanders, Jr. (eds.), EMAS Publishers, U. K., 321-337, (1986).

2. M. E. Fine, "Precipitation Hardening of Aluminum Alloys", Met. Trans. 6A, 625-630, (1975).

3. C. M. Adam, "Structure/Property Relationships and Applications of Rapidly Solidified Aluminum Alloys", in Rapidly Solidified Amorphous and Crystalline Alloy, B. H. Kear, B. C. Giessen and M. Cohen, editors, Elsevier Science Publishing Co., Inc., 411-422 (1982).

4. N. Ryum, "Precipitation and Recrystallization In An Al-0.5 wt.% Zr-Alloy", Acta Metall. vol. 17, 269-278, (1969).

5. O. Izumi and D. Oelschlagel, "On the Decomposition of a Highly Supersaturated Al-Zr Solid Solution", Scripta Metall. 3, 619-622, (1969).

6. E. Ness, "Precipitation of the Metastable Cubic Al_3Zr-Phase in Subperitectic Al-Zr Alloys", Acta Metall. 20, 499-506, (1972).

7. M. S. Zedalis, "Development of an Elevated Temperature Aluminum Alloy containing Al X-Type Dispersed Phases", PhD Thesis, Northwestern University, (1985).

8. Y. C. Chen, M. E. Fine, J. R. Weertman and R. E. Lewis, "Coarsening Behavior of Ll_2 Structured $Al_3(Zr_xV_{1-x})$ Precipitates in Rapidly Solidified Al-Zr-V Alloy", Scripta Metall. 21, 1003-1008, (1987).

9. R. E. Lewis, D. D. Crooks, Y. C. Chen, M. E. Fine and J. R. Weertman, "High Temperature Al-Zr-V Alloys Using Rapid Solidification Processing" in Proceedings of 3rd Int. Conf. on Creep and Fracture of Engineering Materials and Structures, B. Wilshire and R. W. Evans (eds.), Institute of Metals, London 331-346, (1987).

10. F. H. Cocks, M. L. Shepard and H. G. Chilton, "An Electrochemical Method for the Extraction of Precipitates from Age-Hardenable Aluminum Alloys", J. of Mater. Sci. 12, 494-496, (1977).

11. Y. C. Chen, PhD dissertation, Northwestern University, Evanston, IL., (1988).

12. E. Nes and H. Billdal, "The Mechanism of Discontinuous Precipitation of the Metastable Al Zr Phase From an Al-Zr Solid Solution", Acta. Met., 25, 1039-1046, (1977).

13. Y. C. Chen, M. E. Fine and J. R. Weertman, MRS Int. Symposium on Advanced Materials, Tokyo, Japan, May 30-June 3, 1988.

14. E. D. Zakharov and G. L. Shneyder, "Volume Effect and Properties of Alloys Solid Solutions of Substitution", Russian Metall., 141-145, (1978).

15. N. I. Varich, L. M. Burov, K. Y. Kolesnichenko and A. P. Maksimenko, "Highly Supersaturated Al-V, Al-Mo and Al-W Solid Solutions Obtained at a High Rate of Cooling", Fiz. Metal. Metalloved., 15, No. 2, 292-295, (1963.).

16. L. M. Burov and A. A. Yakunin, "Effect of the Rate of Cooling on the Composition of Solid Solutions in Binary Alloys Based pn Aluminum", Russian J. of Physical Chemistry, 42, 540-541, (1968).

17. P. W. Voorhees and M. E. Glicksman, "Ostwald Ripening During Liquid Phase Sintering -- Effect of Volume Fraction on Coarsening Kinetics", Met. Trans. 15A, 1081-1088, (1984).

18. P. K. Footner and B. P. Richards, "Long-Term Growth of Superalloy Particles", J. of Mater. Sci. 17, 2141-2153, (1982).

19. A. J. Ardell and R. B. Nicholson, "The Coarsening of r'in Ni-Al Alloys", J. Phys. Chem. Solids, 27, 1793-1804, (1966).

20. D. B. Williams and J. W. Edington, "The Precipitation of ' (Al_3Li) in dilute Aluminum Lithium Alloys", J. Metal Sci. 9, 529-532, (1975).

21. T. Marumo, S. Fujikawa and Ken-ichi Hirano, "Diffusion of Zirconium in Aluminum", J. Japan Inst. Light Metals 23, 17-25, (1973).

22. W. L. Fink, and L. A. Willey, "Equilibrium Relations in Aluminum - Zirconium Alloys of High Purity", Trans. AIME vol. 133, 69-80, (1939).

23. M. F. Ashby, C. Gandhi and D. M. R. Taplin, "Fracture-Mechanism Maps and Their Construction for FCC Metals and Alloys", Acta Metall. 27, 699-729, (1979).

24. B. Reppich, H. Bugler, R. Leistner and M. Schutze, "Application of the Microstructural Concept of Creep and Rupture Life Time to A Precipitating Ni-Base Alloy-I. Yielding and Creep Behavior", Proc. of the 2nd Int. Conf. on "Creep and Fracture of Engineering Materials and Structures", Swansea, 279-297, (1984).

25. P. J. Henderson and M. McLean, "Microstructural Contributions to Friction Stress and Recovery Kinetics During Creep of the Nickel-Base Superalloy IN738LC", Acta Metall. 31, 1203-1219, (1983).

26. R. W. Lund and W. D. Nix, "High Temperature Creep of Ni-20Cr-2ThO Single Crystals", Acta Metall. 24, 469-481, (1976).

27. J. Lin and O. D. Sherby, "Creep of Oxide Dispersion Strengthened Materials (with Special Reference to T-D Nichrome)", Res Mech. 2, 251-293, (1981).

28. M. McLean, "On the Threshold Stress for Dislocation Creep in Particle Strengthened Alloys", Acta Metall. 33, 545-556, (1985).

29. A. K. Mukherjee, J. E. Bird and J. E. Dorn, "Experimental Correlations for High-Temperature Creep", Am. Soc. Metal. Trans. 62, 155-179, (1969).

30. O. D. Sherby, R. H. Klundt and A. K. Miller, Met. Trans. 8A, 843-850, (1977).

Table 1 Nominal compositions of three Al-Zr-V alloys.

Alloy	Composition (wt.%)
2	Al-3.12 Zr-0.66 V
3	Al-2.14 Zr-1.24 V
4	Al-1.13 Zr-1.82 V

Table 2 Measured volumetric coarsening rate constants K and coefficients of linearity R for Ll_2 $Al_3(Zr_{.25}V_{.75})$ precipitates in alloy 4 aged at 425, 450, and 500°C.

Temperature (°C)	K (m^3/hr)	R
425*	1.03×10^{-28}	0.997
450*	6.13×10^{-28}	0.997
500	1.28×10^{-26}	0.996

* Specimens were preaged at 500°C for 2.5 hours to prevent cellular precipitation.

Table 3 Tensile properties of extruded alloys 2 and 4 tested at 425°C, in Ar.

Alloy	Yield Stress* (0.2% offset) MPa	Ultimate Tensile** Strength MPa	Elongation %
2	13.8	22.0	16.5
4	42.7	66.8	21.8

* measured with $\dot{\epsilon} = 1 \times 10^{-4}$/sec.

** measured with $\dot{\epsilon} = 1 \times 10^{-3}$/sec.

epsilon, dot

Table 4 Calculated change of lattice constant, Δa, of supersaturated solid solutions of Al-Zr-V alloys from that of unalloyed Al.

Alloy	Δa (Å)* (from Zr)	Δa (Å)** (from V)	Δa (Å) (total)
2. Al-3.50wt%Zr -0.54wt%V	+0.0175	-0.0016	+0.0159
3. Al-2.15wt%Zr -1.22wt%V	+0.0108	-0.0037	+0.0071
4. Al-1.16wt%Zr -1.76wt%V	+0.0058	-0.0053	+0.0005

* $\Delta a/wt\%Zr = +0.005$ Å/wt%

** $\Delta a/wt\%V = -0.0033$ Å/wt%

FIGURE CAPTIONS

Figure 1 Dimensions (in mm) of specimens (a) S1 and (b) S2.

Figure 2 Optical micrographs of cross section of as-melt-spun alloy 4 ribbon at areas (a) with flat chill surface and (b) with uneven chill surface. Chill surfaces at bottom, free surfaces at top.

Figure 3 Typical TEM microstructures of (a) alloy 2, (b) alloy 3, and (c) alloy 4 ribbons in the as-melt spun condition.

Figure 4 TEM dark field micrographs from as-spun alloy 2 ribbon, where (a) was taken operating with [110] spot of the Ll_2 phase, and (b) was taken operating with [111] spot of the "Q" phase.

Figure 5 Alloy 4 ribbon aged at 350°C for 3 hours.

Figure 6 High resolution electron micrograph of an $Al_{10}V$ particle.

Figure 7 High resolution electron micrograph of an Ll_2 phase particle in Al matrix from alloy 4 ribbon aged at 600°C for 1.5 hours.

Figure 8 Growth kinetics of Ll_2 $Al_3(Zr_{.25}V_{.75})$ at various temperatures in alloy 4 ribbon. A pre-aging of 2.5 hours at 500°C was done for the specimens aged at 425 and 450°C.

Figure 9 Ll_2-structured $Al_3(Zr_{.25}V_{.75})$ particles in alloy 4 ribbon after aging at 500°C for (a) 20, and (b) 206 hours.

Figure 10 Optical micrograph of as-extruded alloy 2. The structural inhomogeneity and the coarse second phase particles are to be noted.

Figure 11 Typical microstructures (TEM) of (a) alloy 2, (b) alloy 3, and (c) alloy 4 after extrusion. Extrusion direction is normal to the micrograph in each case.

Figure 12 Creep curves of three extruded Al-Zr-V alloys tested at 425°C with an initial stress of 17 MPa.

Figure 13 SEM fractograph from alloy 2 after being crept at 425°C with σ_i = 17 MPa. A dimple structure is shown.

Figure 14 (a) SEM fractograph from alloy 4 after being crept at 425°C with σ_i = 17 MPa. (b) Higher magnification of left-hand edge, and (c) higher magnification of right-hand edge.

Figure 15 Dark field TEM micrograph from alloy 4 after being crept at 425°C. It shows shearing of Ll_2 phase particles by dislocations resulting in formation of faults.

Figure 16 Plot on log-log scale of normalized creep rate $\dot{\epsilon}_s kT/DGb$ versus normalized creep stress σ/G , for alloy 4.

Figure 17 Determination of the activation energy for the coarsening of the Ll_2-structured $Al_3(Zr_{.25}V_{.75})$ by a plot of ln(KT) vs 1/T.

Figure 18 Comparison at various stresses of the creep rate obtained from alloy 4 with the values predicted from equation (8) with σ_o equal to 14.2 MPa (curve 1), and equation (9) with σ_{th} equal to 8.7 MPa (curve 2).

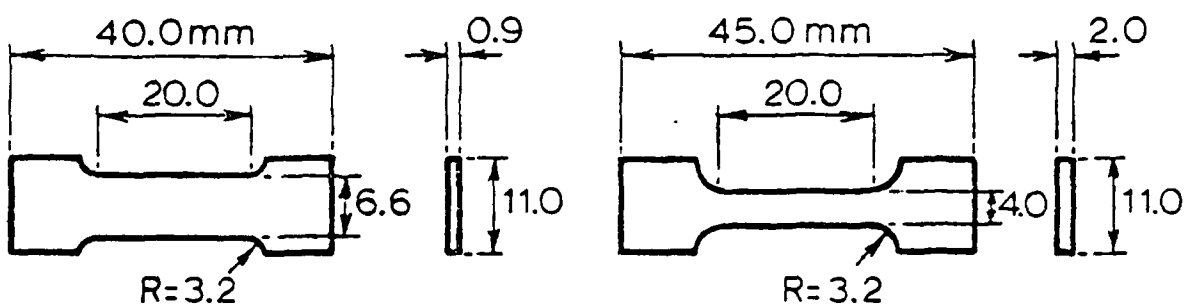

Figure 1 Dimensions (in mm) of specimens (a) S1 and (b) S2.

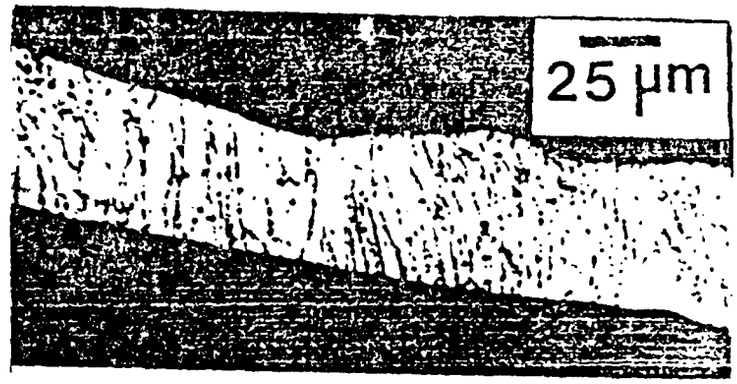

a

b

Figure 2 Optical micrographs of cross section of as-melt-spun alloy 4 ribbon at areas (a) with flat chill surface and (b) with uneven chill surface. Chill surfaces at bottom, free surfaces at top.

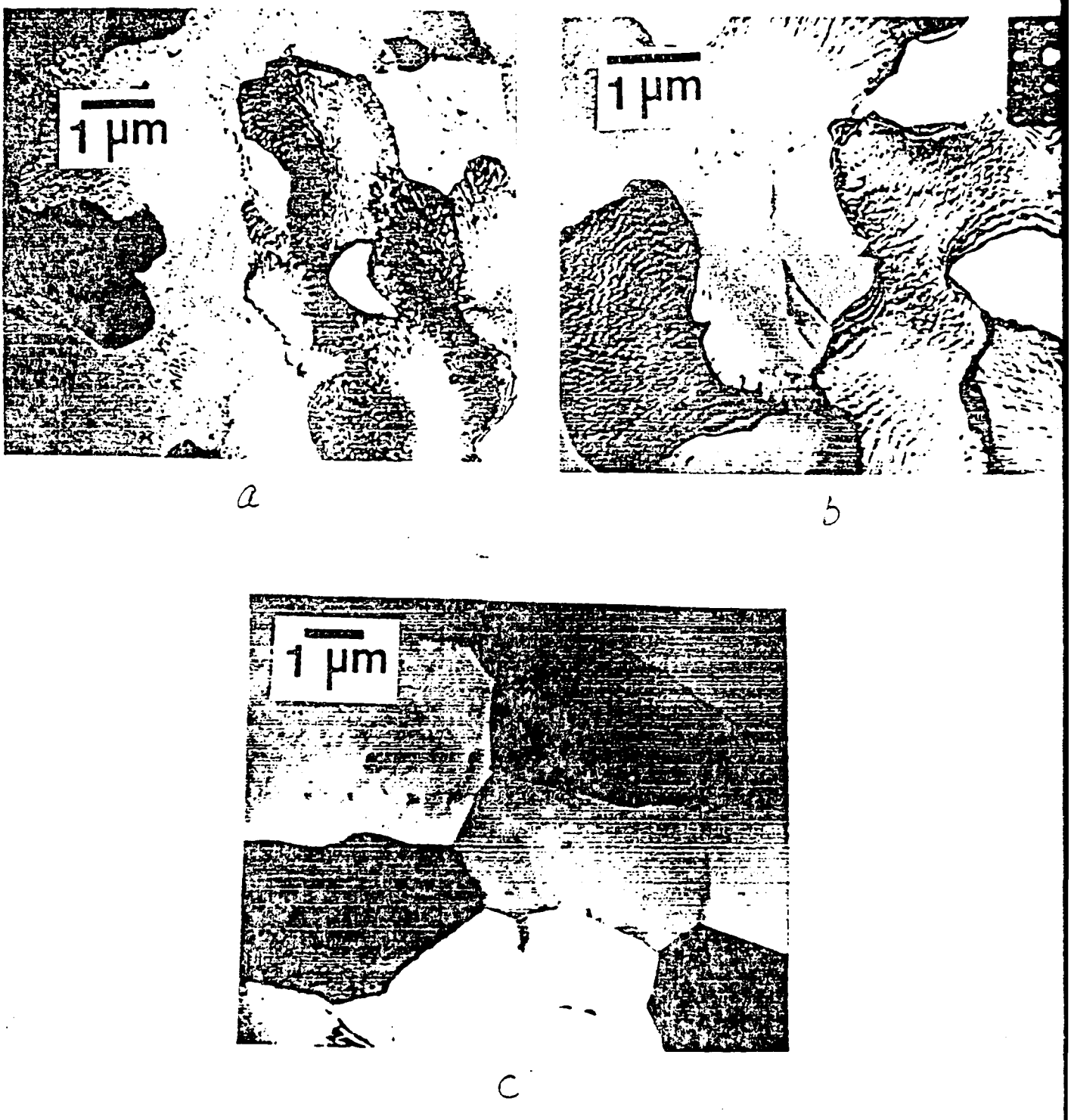

Figure 3 Typical TEM microstructures of (a) alloy 2, (b) alloy 3, and (c) alloy 4 ribbons in the as-melt spun condition.

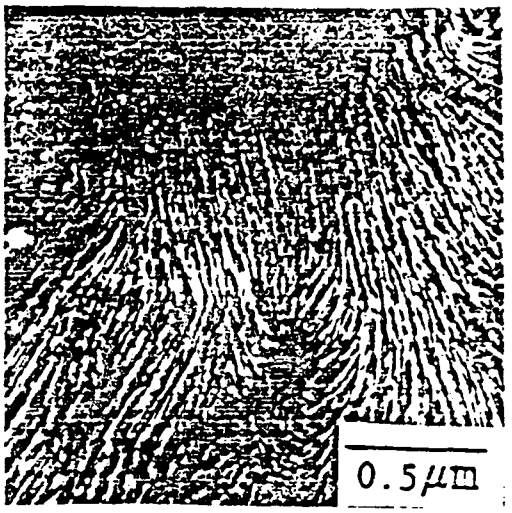

a

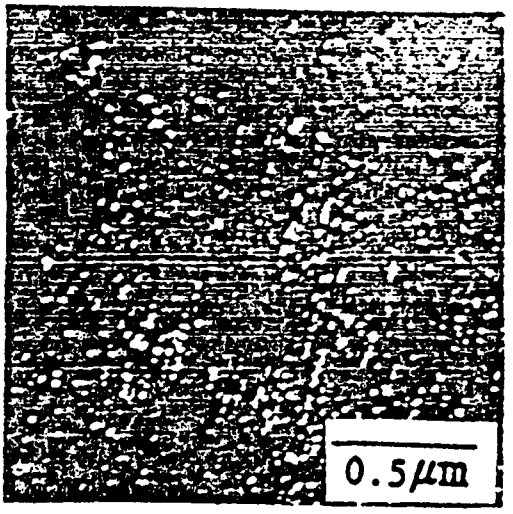

b

Figure 4 TEM dark field micrographs from as-spun alloy 2 ribbon, where (a) was taken operating with [110] spot of the $L1_2$ phase, and (b) was taken operating with [111] spot of the "Q" phase.

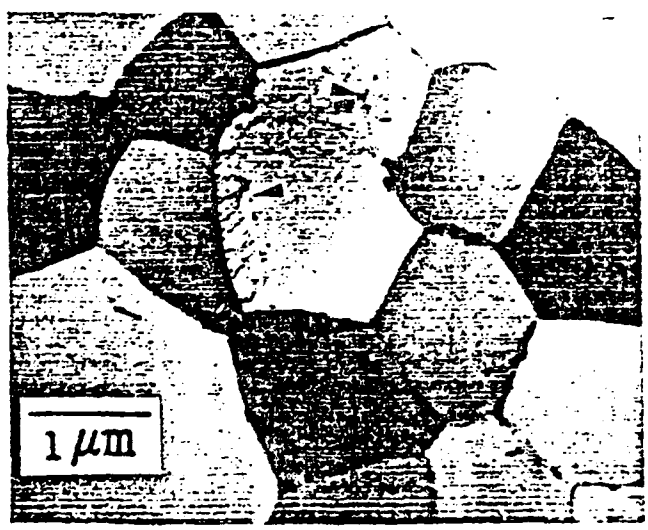

Figure 5 Alloy 4 ribbon aged at 350°C for 3 hours.

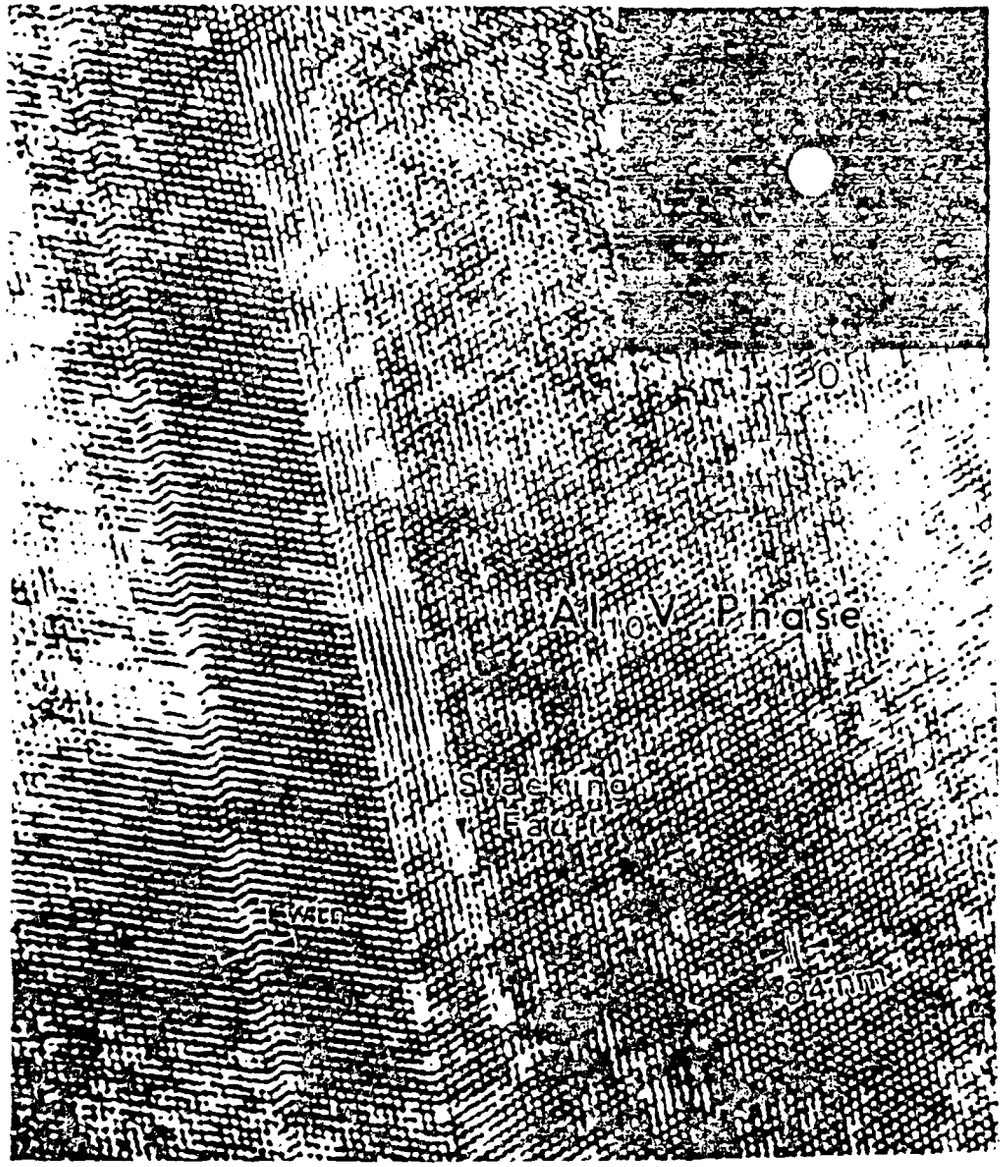

Figure 6 High resolution electron micrograph of an $Al_{10}V$ particle.

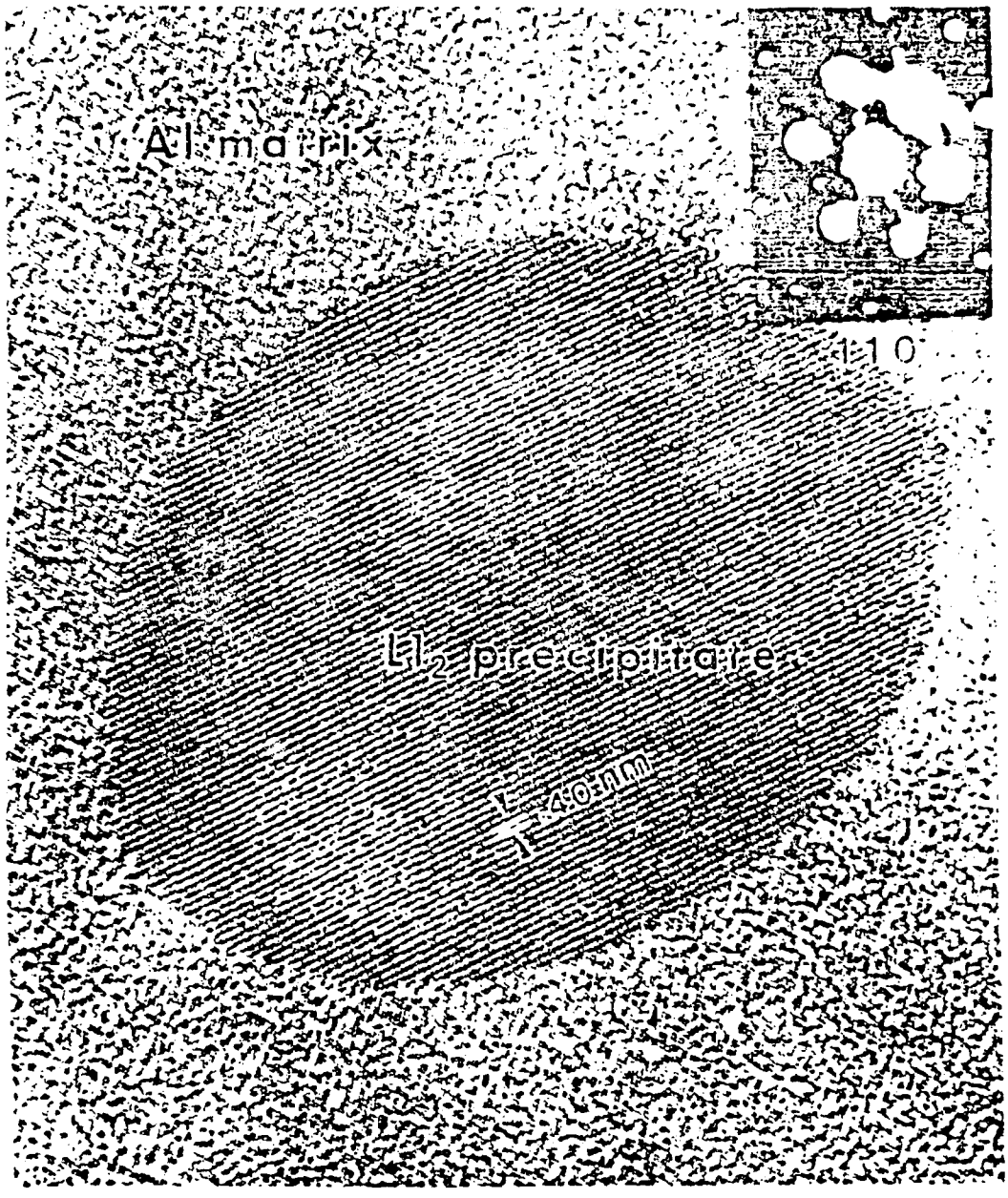

Figure 7 High resolution electron micrograph of an $L1_2$ phase particle in Al matrix from alloy 4 ribbon aged at 600°C for 1.5 hours.

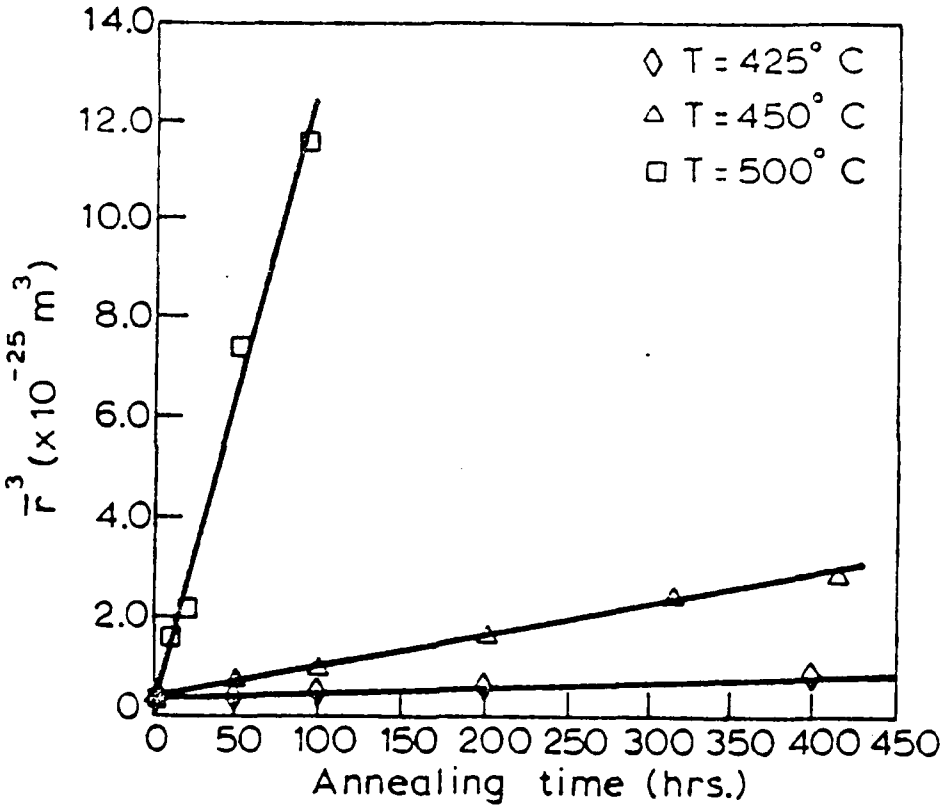

Figure 8 Growth kinetics of Ll_2 $Al_3(Zr_{.25}V_{.75})$ at various temperatures in alloy 4 ribbon. A pre-aging of 2.5 hours at 500°C was done for the specimens aged at 425 and 450°C.

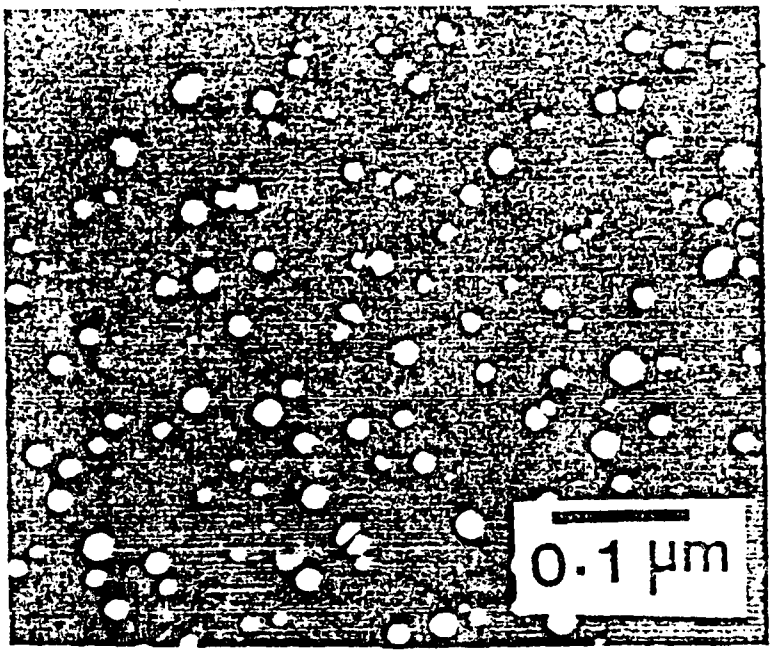

a

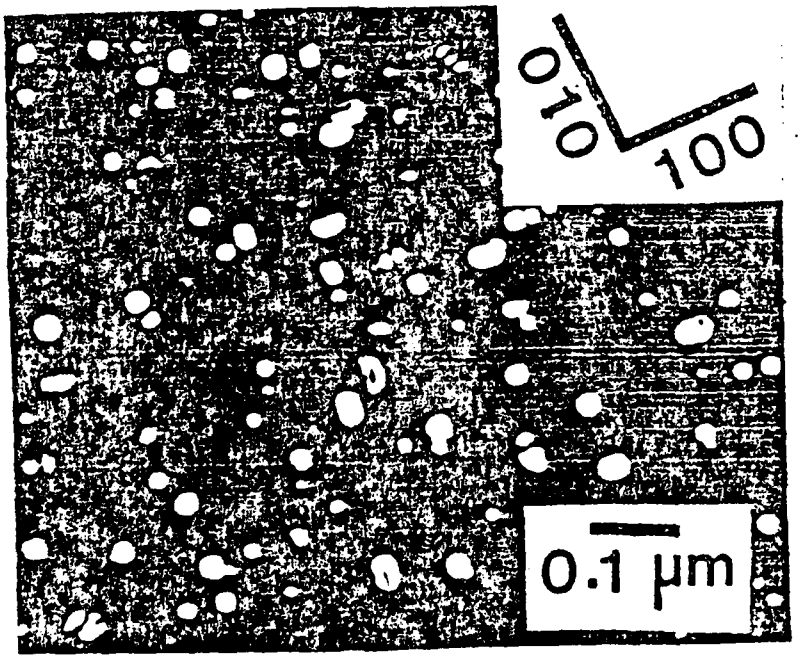

b

Figure 9 $L1_2$-structured $Al_3(Zr_{.25}V_{.75})$ particles in alloy 4 ribbon after aging at 500°C for (a) 20, and (b) 206 hours.

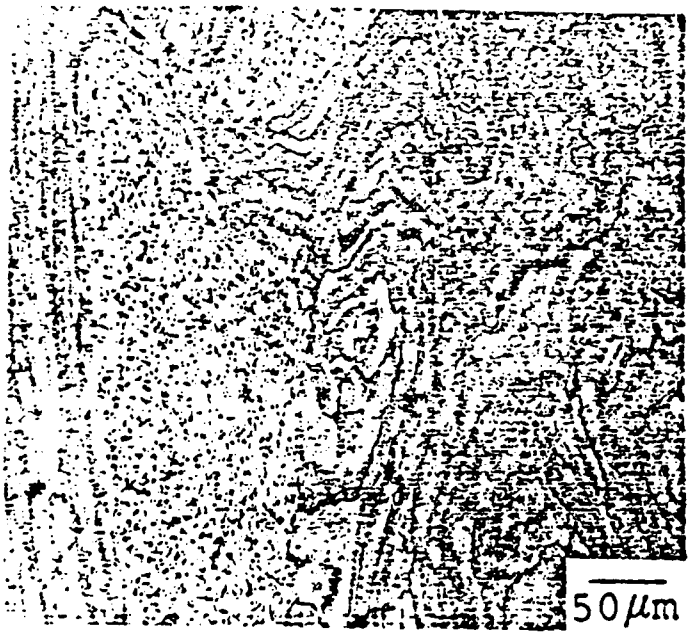

Figure 10 Optical micrograph of as-extruded alloy 2. The structural inhomogeneity and the coarse second phase particles are to be noted.

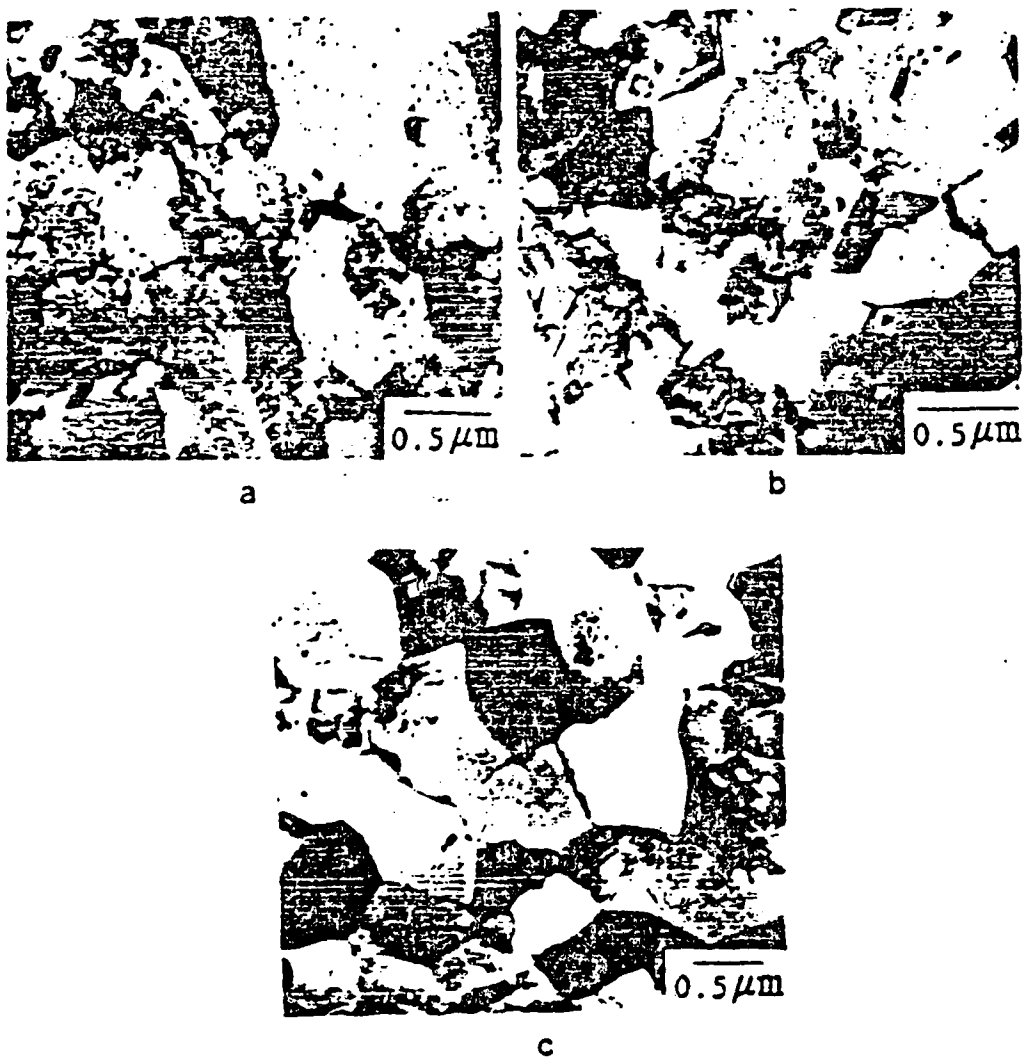

Figure 11 Typical microstructures (TEM) of (a) alloy 2, (b) alloy 3, and (c) alloy 4 after extrusion. Extrusion direction is normal to the micrograph in each case.

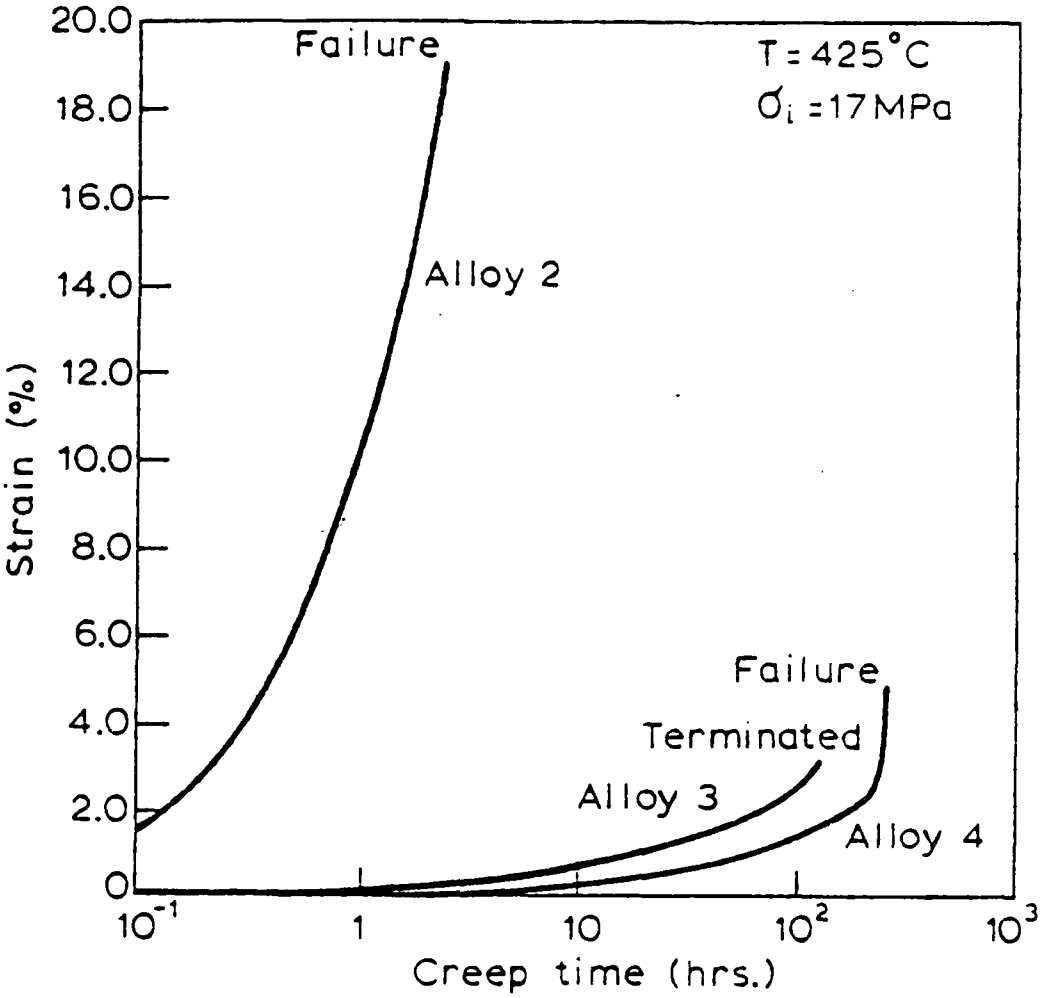

Figure 12 Creep curves of three extruded Al-Zr-V alloys tested at 425°C with an initial stress of 17 MPa.

Figure 13 SEM fractograph from alloy 2 after being crept at 425°C with σ_1 = 17 MPa. A dimple structure is shown.

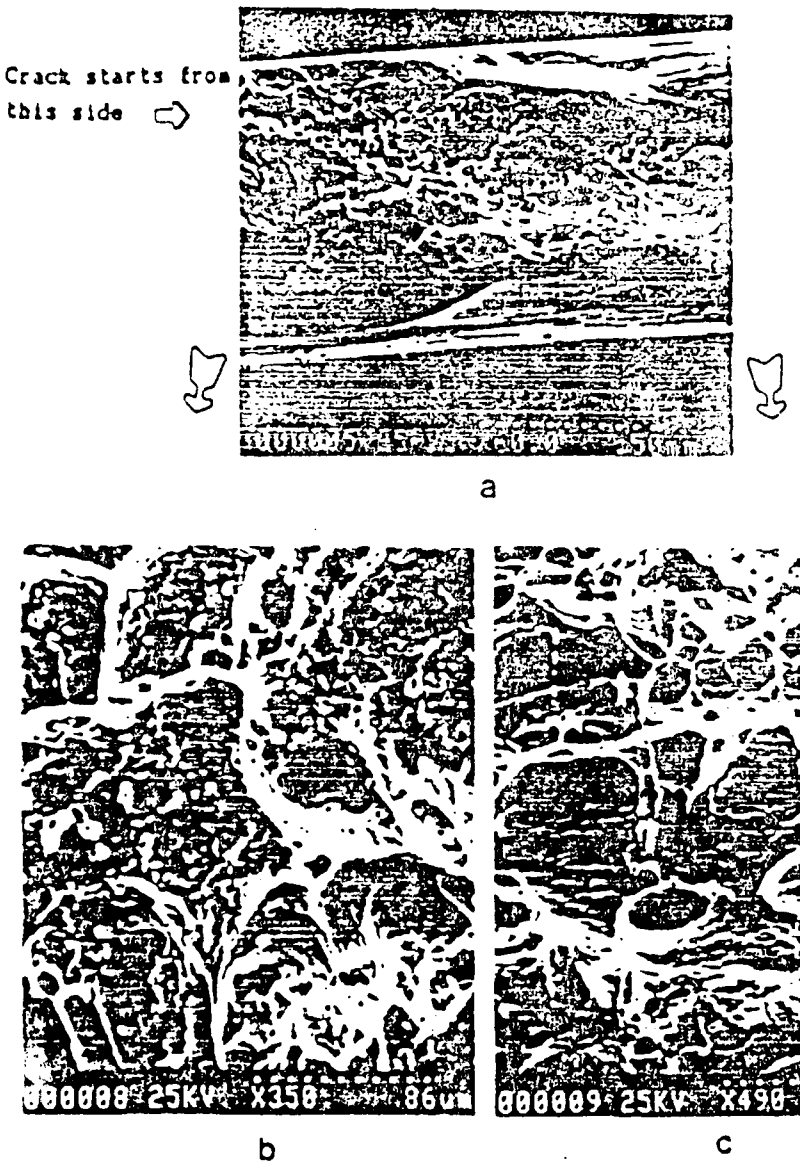

Figure 14 (a) SEM fractograph from alloy 4 after being crept at 425°C with σ_i = 17 MPa. (b) Higher magnification of left-hand edge, and (c) higher magnification of right-hand edge.

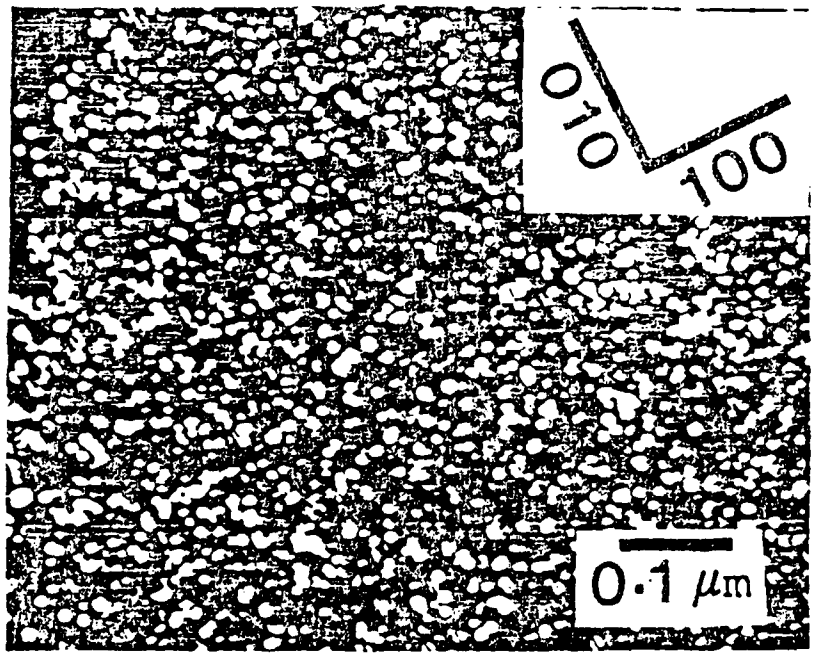

Figure 15 Dark field TEM micrograph from alloy 4 after being crept at 425°C. It shows shearing of Ll_2 phase particles by dislocations resulting in formation of faults.

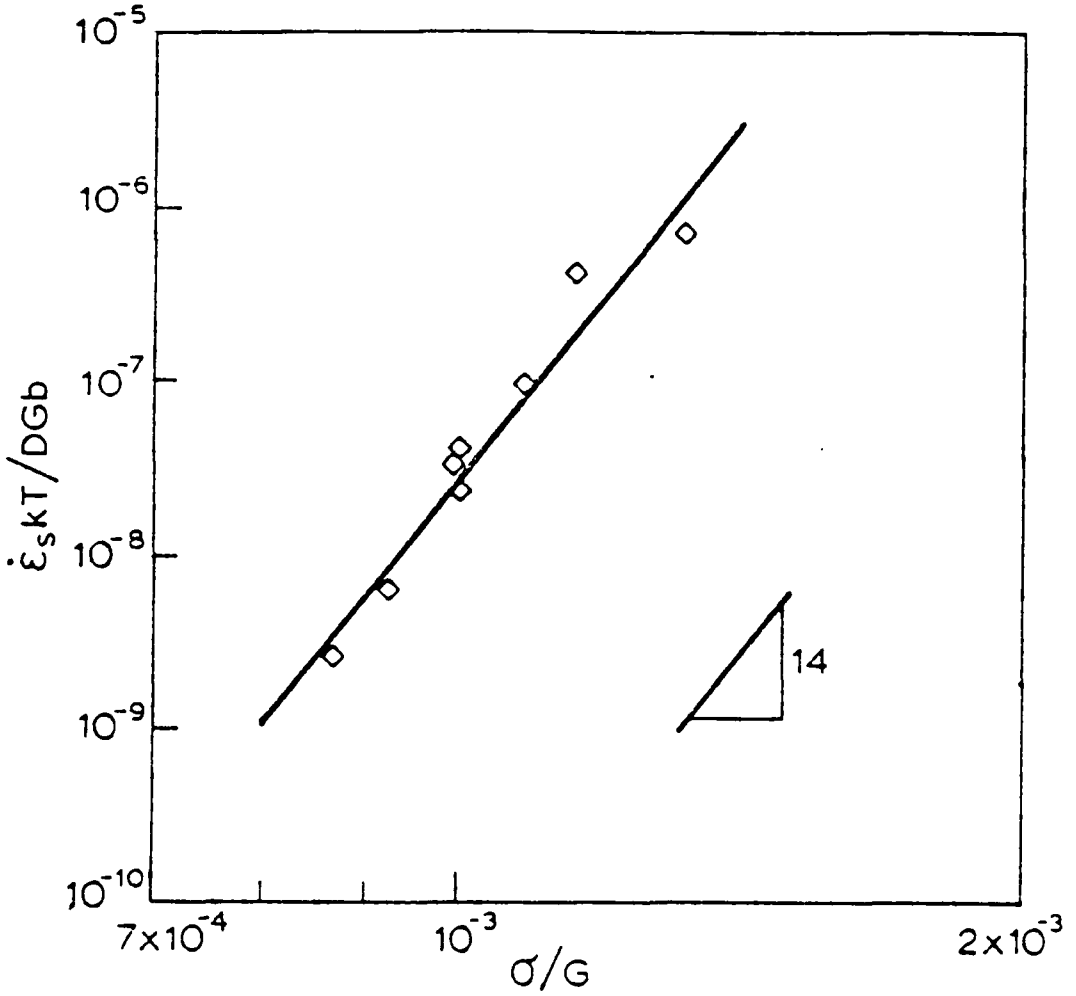

Figure 16 Plot on log-log scale of normalized creep rate $\dot{\epsilon}_s kT/DGb$ versus normalized creep stress σ/G , for alloy 4.

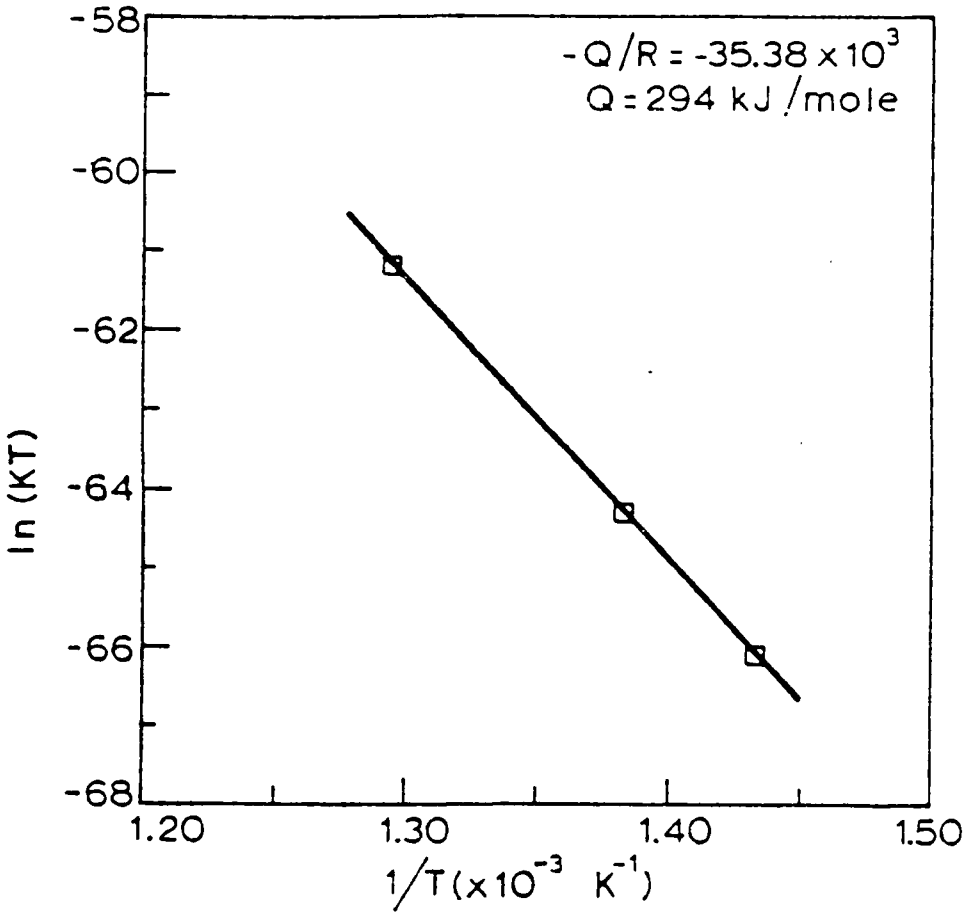

Figure 17 Determination of the activation energy for the coarsening of the Ll_2-structured $Al_3(Zr_{.25}V_{.75})$ by a plot of ln(KT) vs 1/T.

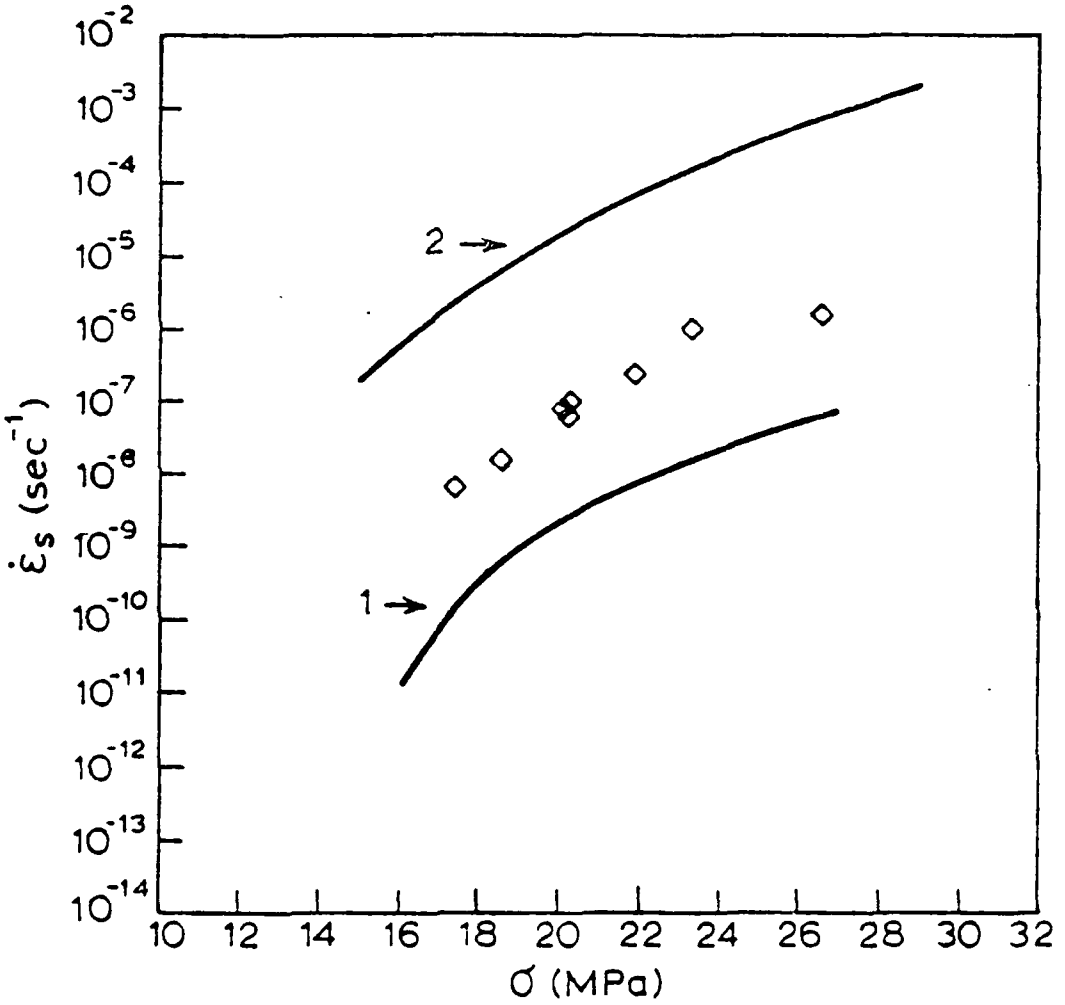

Figure 18 Comparison at various stresses of the creep rate obtained from alloy 4 with the values predicted from equation (8) with σ_o equal to 14.2 MPa (curve 1), and equation (9) with σ_{th} equal to 8.7 MPa (curve 2).

APPENDIX C

To appear in January 1985 issue of Scripta Metallurgica

COARSENING BEHAVIOR OF $L1_2$ PHASE IN AN Al-Zr-Ti ALLOY

V. R. Parameswaran*, J. R. Weertman and M. E. Fine
Department of Materials Science and Engineering
Northwestern University, Evanston, IL 60208

Introduction

Aluminum alloys with improved high temperature mechanical properties are of particular interest to aerospace applications because of their low densities and high strength-to-weight ratios, and their resistance to corrosion and oxidation. By analogy with the γ'-strengthened nickel base superalloys, which remain stable and retain their useful strengths up to 0.73 T_m (where T_m is the absolute melting temperature), development of a dispersion strengthened aluminum alloy useful to 425°C seems to be an achievable target. Development of such alloys is an active field of research (1,2).

For stable mechanical behavior, the dispersed phase should resist phase transformation a growth by Ostwald ripening. A basic requirement for resistance to growth of the dispersed phase is low interfacial energy between dispersoid and matrix. Irrespective of the controlli mechanism, reduction in the total interfacial energy governs the growth of the particles.

A class of alloys based on Al-Zr is under investigation at Northwestern University. Addi tion of a third element such as V, Ti or Hf was found to improve the lattice matching between the tetragonal DO_{23}-structured dispersoid and the matrix (3,4). The alloy Al-Zr-V, in partic lar, has been studied extensively (5-9). Metastable $L1_2$-structured second phase dispersoids $Al_3(Zr_xV_{1-x})$, with x varying between 0.125 and 0.875, form in rapidly solidified solid solutio Al-Zr-V. The $L1_2$ particles, which have the same cubic structure as γ' in nickel base superalloys, grow only slowly at high temperatures. Thus they provide a stable strengthening to th alloy. The $L1_2$ precipitates are spherical in shape. They are coherent and coplanar with the matrix. At very high temperatures, or long times at 425°C, the metastable $L1_2$ dispersoids are replaced by the equilibrium phases, DO_{23}-structured $Al_3(Zr,V)$ and complex cubic $Al_{10}V$ (9). In alloys with 5 vol.% of $L1_2$-structured $Al_3(V_{.75}Zr_{.25})$, incoherent $Al_{10}V$ forms at the grain boundaries and creates precipitate free zones (PFZ) in the adjacent matrix. The PFZs become an increasing problem as the amount of V is increased in the alloy. The growth of PFZs is a function of aging time and temperature (9).

From this point of view Al-Zr-Ti alloys are more promising since the stable tetragonal phase in this system matches the Al lattice rather well and it is not expected to form at grai boundaries as readily as does $Al_{10}V$. Thus it is of interest to compare the rate of Ostwald ripening of $L1_2$-structured $Al_3(Zr,Ti)$ with that of $Al_3(Zr,V)$. Alloys containing 1 vol.% of $Al_3(Zr_{.75}Ti_{.25})$ were prepared, and the growth of the $L1_2$-structured precipitates during high temperature aging was studied. This paper reports the results.

Experimental Procedure

Small quantities (about 4 g) of alloys formulated to contain 1 vol.% of $Al_3(Zr_{.75}Ti_{.25})$ were arc melted under argon atmosphere using a water cooled copper crucible and a non-consumable tungsten electrode. This procedure was followed in previous studies of Al-Zr-V (5,7).

* Presently with National Aeronautical Establishment, National Research Council Canada, Ottawa, Ontario K1A 0R6, Canada.

The nominal composition of the alloy was: 99.62 wt.% Al, 0.08 wt.% Zr, and 0.3 wt.% Ti. The microstructure of the as-cast alloy did not show any precipitates on the chilled side of the cast buttons, indicating that the solutes were in metastable solid solution in the aluminum.

Thin slices (about 0.5 mm in thickness) were cut from the buttons using a diamond saw. These slices were given a pre-aging treatment at 500°C for one hour in order to prevent cellular precipitation during subsequent aging. Pre-aging to prevent cellular precipitation was used previously with arc melted Al-Zr-V alloys containing 1 vol.% of Ll_2 precipitates (5,7). The pre-aged samples were held at 425°C for different times up to 600 hours. All aging was carried out under vacuum (better than 10^{-3} Pa); the temperature was maintained at 425 ± 1°C.

After aging, 3 mm diameter discs were cut from the slices using an electrodischarge machine. The discs were first mechanically polished down to a thickness of about 0.05 mm, and then subjected to double jet electropolishing to produce thin foils for transmission electron microscopy studies. The electrolyte used was a 25% solution of nitric acid in anhydrous methanol. Temperature during electropolishing was -50°C, and the current density was about 95 mA. The polished foils were examined in a 200 kV Hitachi 700-H electron microscope operated at 175 kV.

Results and Discussion

Figure 1 shows the Ll_2 spherical precipitates after aging at 425°C for 200, 400, and 600 hours. Figure 2 compares the variation of particle radius as a function of aging time in the present alloy with that observed earlier by Zedalis (5,7) in the Al-Zr-V alloy containing 1 vol.% Al ($Zr_{.125}V_{.875}$).

The precipitate sizes in the present Al-Zr-Ti alloy are much smaller than those observed in Al-Zr and Al-Zr-V alloys prepared under conditions thought to be identical. The scatter in the precipitate sizes increased with increasing aging times; however, even the largest particles in the Al-Zr-Ti alloy, after aging for 600 hours at 425°C, are smaller than average size in the Al-Zr-V alloy after 400 hours aging. (In the previous study (5,7), aging was not done beyond 400 hours.) Some particles grew faster than others. This may be due to enhanced diffusion along dislocations. Note in Fig. 1, especially 1c, that some particles are near or are attached to dislocations. These particles are especially large. Also, an inhomogeneous distribution of solute plays a role. Many precipitates in Fig. 1b appear to be along bands, and the particle radii seem to be larger here than those not on bands in this micrograph.

Chen (9) observed that the particle sizes and their growth rates were smaller in rapidly solidified Al-Zr-V alloys (splats and melt spun ribbons) containing 5 vol.% dispersoids than in the 1 vol.% arc cast alloys. These differences in particle sizes and growth rates were attributed to non-uniform distribution of solutes in the arc cast alloys (9).

Because the Ll_2 particle sizes appear to be smaller in an Al-Zr-Ti alloy than in a similar Al-Zr-V alloy while the particle growth rates at 425°C are comparable, and because the harmful grain boundary particles such as $Al_{10}V$ are absent in the Al-Zr-Ti alloys, this latter seems to be the more promising system for high temperature applications. Further investigation is planned of Al-Zr-Ti alloys prepared by melt spinning. These alloys contain higher volume fractions of dispersoids.

Acknowledgements

This research was supported by the Air Force Office of Scientific Research Grant No. AFOSR-85-0337 under the direction of Dr. Alan H. Rosenstein. The use of the facilities of Northwestern University's Materials Research Center supported under the NSF-MRL program (Grant No. DMR8520280) is gratefully acknowledged.

References

1. M. E. Fine, in Dispersion Strengthened Aluminum Alloys, edited by Y. W. Kim and W. N. Griffiths, The Metallurgical Society, Warrendale, PA. In press.
2. L. Angers, Y. Chen, M. E. Fine, J. R. Weertman and M. S. Zedalis, in Aluminum Alloys, Their Physical and Mechanical Properties, edited by E. A. Starke, Jr. and T. M. Sanders, Jr., Vol. I, Engineering Materials Advanced Services Ltd., U.K., pp. 321-337.
3. S. Tsunekawa and M. E. Fine, Scripta metall. 16, 391 (1982).
4. M. Zedalis and M. E. Fine, Scripta metall. 17, 1247 (1983).
5. M. Zedalis and M. E. Fine, Metall. Trans. A, 17A, 2187 (1986).

6. R. E. Lewis, D. D. Crooks, Y. C. Chen, M. E. Fine and J. R. Weertman, in Proceedings of the Third International Conference on Creep and Fracture of Engineering Materials and Structures, edited by B. Wilshire and R. W. Evans, Institute of Metals, London, 1987, pp. 331-346.
7. M. Zedalis, Ph.D. Thesis, Northwestern University, Evanston, IL, 1985.
8. Y. C. Chen, M. E. Fine, J. R. Weertman and R. E. Lewis, Scripta metall. 21, 1003 (1987).
9. Y. C. Chen, Ph.D. Thesis, Northwestern University, Evanston, IL, 1988.

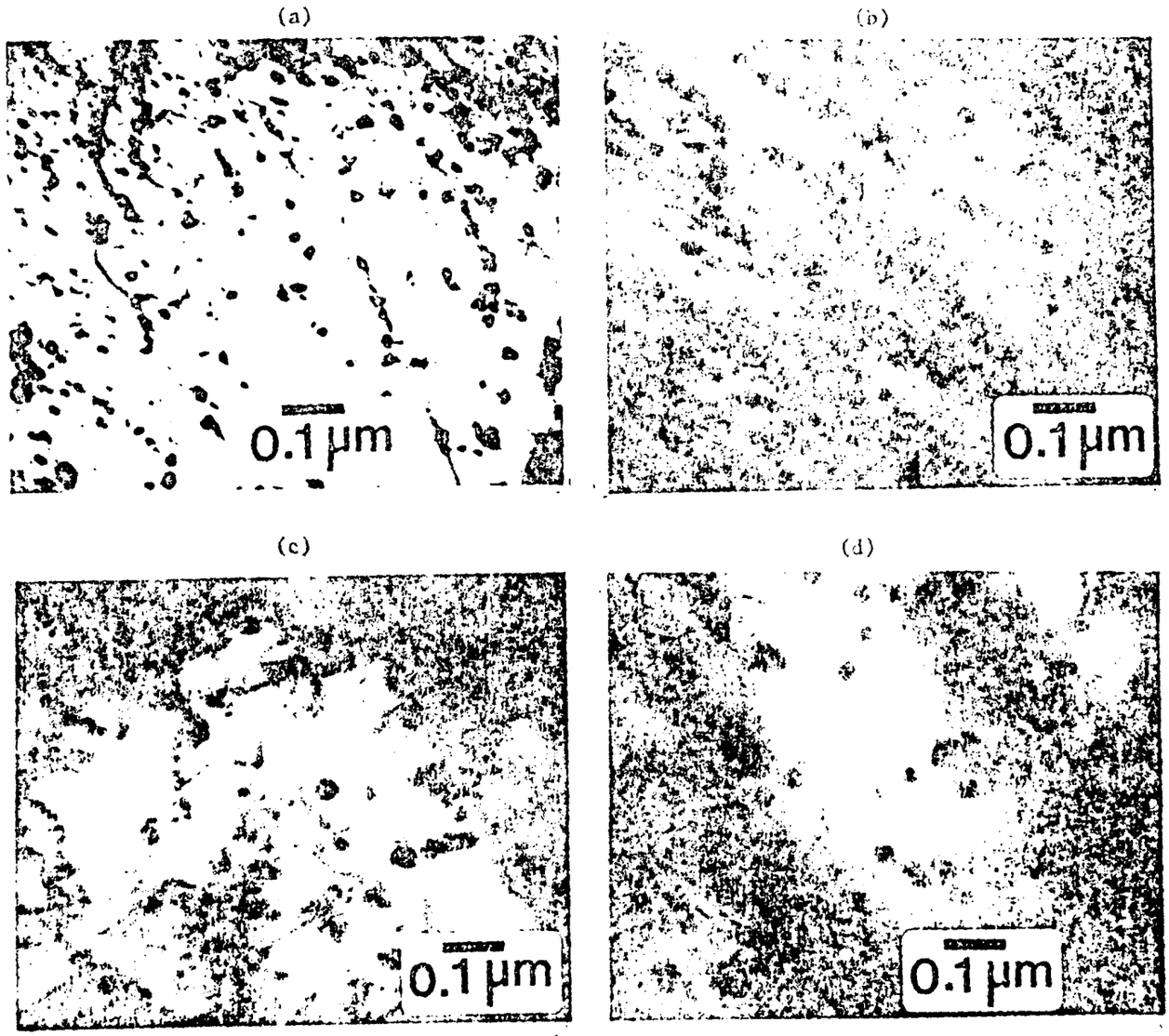

FIG. 1

$L1_2$ precipitates in an Al-Zr-Ti alloy containing 1 vol.% $Al_3(Zr_{.75}Ti_{.25})$ after aging for various times. All samples were pre-aged at 500°C for one hour.

(a) 200 hours, (b) and (c) 400 hours, and (d) 600 hours

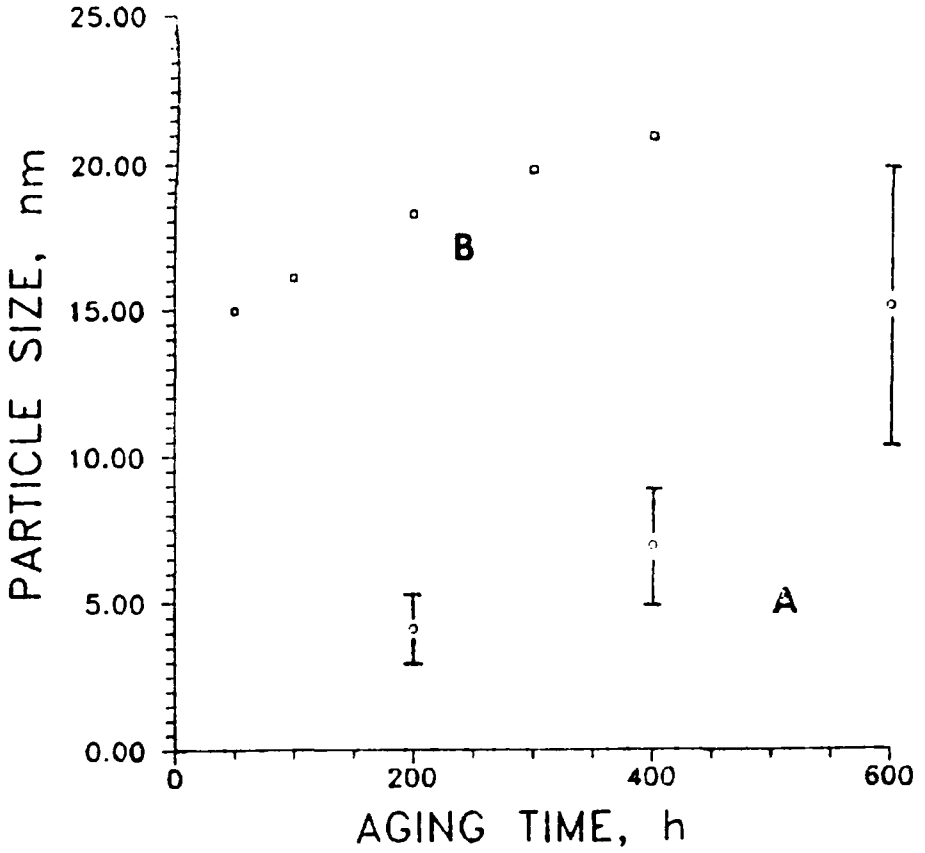

FIG. 2

Variation of Ll_2 average particle radius, $\bar{r}$, with aging time at 425°C.

A: Present results in Al-1 vol.% $Al_3(Zr_{.75}Ti_{.25})$, arc melted.
B: Al-1 vol.% $Al(Zr_{.125}V_{.875})$, arc melted. From (5,7).

All samples were pre-aged at 500°C for one hour.